# ESA Climate Change Initiative (CCI+)
Essential Climate Variable (ECV)

Antarctica_Ice_Sheet_cci+ (AIS_cci+)

Product Validation and Intercomparison Report (PVIR)

Prime & Science Lead: Andrew Shepherd

University of Leeds, Leeds, United Kingdom

a.shepherd@leeds.ac.uk

Technical Officer: Marcus Engdahl

ESA ESRIN, Frascati, Italy

Marcus.Engdahl@esa.int

Consortium: DTU Microwaves and Remote Sensing Group (DTU-N)

DTU Geodynamics Group (DTU-S)

ENVironmental Earth Observation GmbH (ENVEO)

Deutsches Zentrum für Luft- und Raumfahrt (DLR) Remote Sensing Technology Institute (IMF)

Science [&] Technology AS (ST)

Technische Universität Dresden (TUDr)

University College London (UCL/MSSL)

University of Leeds, School of Earth and Environment (UL)
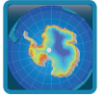
Signatures page
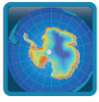
Prepared by	Andreas Groh, TuDr	Date: 01 October 2021
Issued by	Daniele Fantin, Project Manager, S[&]T	Date: 06 October 2021
Checked by	Andrew Shepherd,Science Leader, UL	Date: 06 October 2021
Approved by	Marcus Engdahl, ESA Technical Officer	Date:

Table of Contents

Change Log

Issue	Author	Affected Section	Change	Status
1.0	A. Groh	All	Document Creation	
1.0	All team	All	Document finalization	Delivered to ESA

Acronyms and Abbreviations

AIS	Antarctic Ice Sheet
ATBD	Algorithm Theoretical Basis Document
ATLAS	Advanced Topographic Laser Altimeter System
CCI	Climate Change Initiative
CFL	Calving Front Location
CRDP	Climate Research Data Package
CS2	CryoSat-2
DEM	Digital Elevation Model
DInSAR	Differential Interferometric Synthetic Aperture Radar
DLR	German Aerospace Center
DTU-S	DTU Geodynamics Group
DTU-N	DTU Microwaves and Remote Sensing Group
ECV	Essential Climate Variable
EO	Earth Observation
ENVEO	ENVironmental Earth Observation GmbH
ESA	European Space Agency
GIA	Glacial Isostatic adjustment
GLL	Grounding Line Location
GMB	Gravimetric Mass Balance
IMBIE	Ice Sheet Mass Balance Inter-comparison Exercise
InSAR	Interferometric Synthetic Aperture Radar
IV	Ice Velocity
IW	Interferometric Wideswath
PUG	Product User Guide
PVIR	Product Validation and Intercomparison Report
RA	Radar Altimetry
S&T	Science and Technology AS
SAR	Synthetic Aperture Radar
SEC	Surface Elevation Change
SOW	Statement of Work
TSX/TDX	TerraSAR-X/TanDEM-X SAR mission
TUDr	Technische Universität Dresden
UCL	University College London
UL	University of Leeds

1 Introduction

1.1 Purpose and Scope

This document contains the Product Validation and Intercomparison Report (PVIR) for the Antarctica_Ice_Sheet_cci (AIS_cci) project for CCI+ Phase 1, in accordance to contract and SoW [AD1 and AD2].

The AIS_cci science team has assessed the ECV products in the Climate Research Data Package. An intercomparison of the ECV products with products from other missions and other R&D initiatives has been carried out.

The PVIR describes the results of the validation and inter-comparison exercises, and quantifies the accuracy of the derived products against the validation data and comparable alternative satellite-based products generated by international projects.

The Product Validation and Inter-comparison Report gives a complete report of the activities executed to assessment of the quality of the generated ECV products and the results achieved.
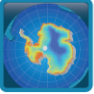
1.2 Document Structure

This document comprises four parts describing each of the parameters of the AIS_cci Essential Climate Variable (ECV). Each parameter has its own chapter as seen below:

- Surface Elevation Change (SEC);
- Ice Velocity (IV);
- Grounding Line Location (GLL);
- Gravimetric Mass Balance (GMB).

Each parameter chapter follows a general structure including

- a description of the requirements for an independent validation data set (Sec. x.1.1)
- a description of available sources of validation data including in-situ observations and alternative data sets (e.g. available products, models, etc.) (Sec. x.1.2)
- a detailed assessment of the validation data including a description of errors and biases as well as uncertainties associated to the data (Sec. x.1.3)
- a description of the selection of validation data sets based on the outlined requirements and assessment of available data (Sec. x.1.4)
- a description of the validation procedure performed on the derived ECV products against the selected validation data sets (Sec. x.2)

- a detailed analysis of the uncertainty of the ECV products with reference to the independent validation data (Sec. x.3)

- recommendations for fixing errors and/or improving the overall product quality (Sec. x.4)

In the interest of brevity, references are given to other project documentation when possible.

1.3 Applicable and Reference Documents

Table 1.1: List of Applicable Documents

No	Doc. Id	Doc. Title	Date	Issue/ Revision/ Version
AD1	ESA/Contract No. 4000126813/19/I-NB	CCI+ PHASE 1- NEW R&D ON CCI ECVS Ice Sheet Antarctica_cci	2019.06.06	
AD2	ESA-CCI-EOPS-PRGM-SOW-18-0118 Appendix 2 to contract.	Climate Change Initiative Extension (CCI+) Phase 1, New R&D on CCI ECVs Statement of Work	2018.05.31	Issue 1 Revision 6

Table 1.2: List of Reference Documents

No	Doc. Id	Doc. Title	Date	Issue/ Revision/ Version
RD1	ST-UL-ESA-AISCCI+-PVP-001	Product Validation Plan (PVP)		
RD2	ST-DTU-ESA-GISCCI+-PMP-001	Product Validation and Inter-comparison Report (PVIR)	2018.05.04	1.3
RD3	ST-UL-ESA-AISCCI+-ATBD-001	Algorithm Theoretical Basis Document (ATBD) for CCI+ Phase 1	2020.03.09	1.0

Note: If not provided, the reference applies to the latest released Issue/Revision/Version

2 Surface Elevation Change (SEC)

This chapter gives a complete report of the activities carried out to assess the quality of the SEC products.

2.1 Independent validation data

2.1.1 Requirements

The data sets used to validate the Surface Elevation Change (SEC) product must have been acquired in Antarctica, be freely available for the project to use, must overlap either fully or partly with the satellite radar altimetry time series used to produce the SEC product, and must be able to be used to measure surface elevation change.

2.1.2 Sources

Airborne Topographic Mapper (ATM) airborne elevation data has been collected in Antarctica on numerous Operation IceBridge campaigns between 1993 and 2019. The validating dataset is the level 4 product, ATM L4 Surface Elevation Rate of Change V001 (Studinger, 2014). This can be obtained free of charge on registration, from https://icebridge.gsfc.nasa.gov/. The surface elevation rate of change in this dataset is calculated from the change in elevations recorded at the same location between two overflights.

2.1.3 Assessment

The airborne validation data sets are produced from data acquired by laser altimeter, therefore it is anticipated that there may be some bias in the validation results because the laser altimeters reflect off the ice surface, whereas the satellite radar altimeters penetrate some depth into the snowpack.

ASIRAS is an airborne radar altimetry instrument that operates at 13.5GHz, the same central frequency as CryoSat-2. This dataset is likely to be subject to similar penetration effects as the satellite radar altimetry data used to produce the SEC product. The level 4 SEC product allows direct comparison of surface elevation change between separate instruments.

It should be noted that the CCI SEC product is calculated over a long, continuous, multiple-mission period, whereas the ASIRAS dataset is acquired during various shorter periods within the limits of the CCI SEC product time periods.

2.1.4 Selection

All available validation data acquired in Antarctica was used to validate the Antarctic CCI SEC product. The data sets used were acquired from 2002 to 2016, which coincides with the Envisat and CryoSat-2 missions. Geographically, most Operation IceBridge campaigns were flown over West Antarctica and the Antarctic Peninsula. Only measurements taken over land were used.
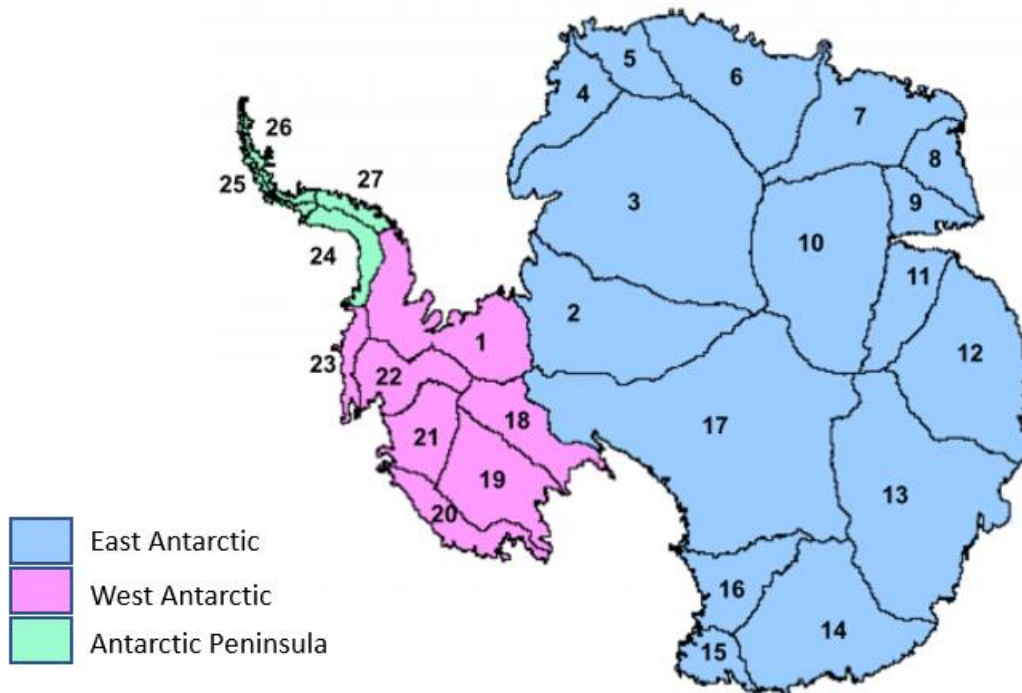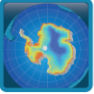
Figure 2-1: Map showing the geographic regions and drainage basins of Antarctica, used during validation of the Antarctic cci surface elevation change product. Drainage basins are based on the Zwally definitions (Zwally et al., 2012). Credit: IMBIE

2.2 Validation procedure

The validation method is a comparison of CCI SEC results with all ASIRAS measurements from the validating dataset that coincide in time and space. This is not a direct comparison to the product dataset, as the ASIRAS overflights are highly irregular. Instead we use the underlying elevation change timeseries and analysis methods from which the CCI SEC dataset was derived to produce results comparable to ASIRAS.

The CCI SEC product is calculated from modelling based on 5km by 5km grid cells in which we derive a series of elevation change values (dh) over time. We can apply a linear least-squares fit over any time period to the dh timeseries in a cell to derive the rate of change of surface elevation, ie dh/dt. For validation we apply the same time periods as ASIRAS to the grid cell timeseries in which ASIRAS took a measurement. We averaged the rates of elevation change computed from pairs of ASIRAS overflights in each cell to match the spatial resolution of the satellite data. The comparison was restricted to where

the root mean square of the ASIRAS results and the standard deviation of the CCI SEC results was less than or equal to 0.4 m/year, and the time period between ASIRAS overflights was at least 2 years. The difference was calculated as CCI SEC minus ASIRAS.

The airborne data is sampled at 250m spatial resolution along flight-lines that preferentially sample fast-thinning ice. Because of this, its measurements tend to be biased to a higher value when compared to coarsely gridded data (Flament and Remy 2012, McMillan 2014). To take account of this, a bias factor is estimated using a high-resolution (1km by 1km) map of ice velocity (Rignot et al 2011a). This bias factor is the velocity of the 1km by 1km grid cell containing the ASIRAS measurement with respect to the average velocity of the 5km by 5km CCI SEC cell containing it, averaged over all measurements used.

The terrain in each drainage basin varies. The CCI SEC product is expected to perform at its best over ice sheets, ie regions of low slope. However, the available comparison data covered many terrains. A comparison covering the whole region was made, as well as separate comparisons for each drainage basin, although it should be noted that the number of datapoints in each basin varies greatly.

2.3 Validation outcome

The differences between the CCI SEC and ASIRAS results over the Antarctic as a whole are shown at cell level in Figure 2-2, below.

Cell-averaged dh/dt comparison to mean-biased ATM

Area: Antarctic Ice Sheets
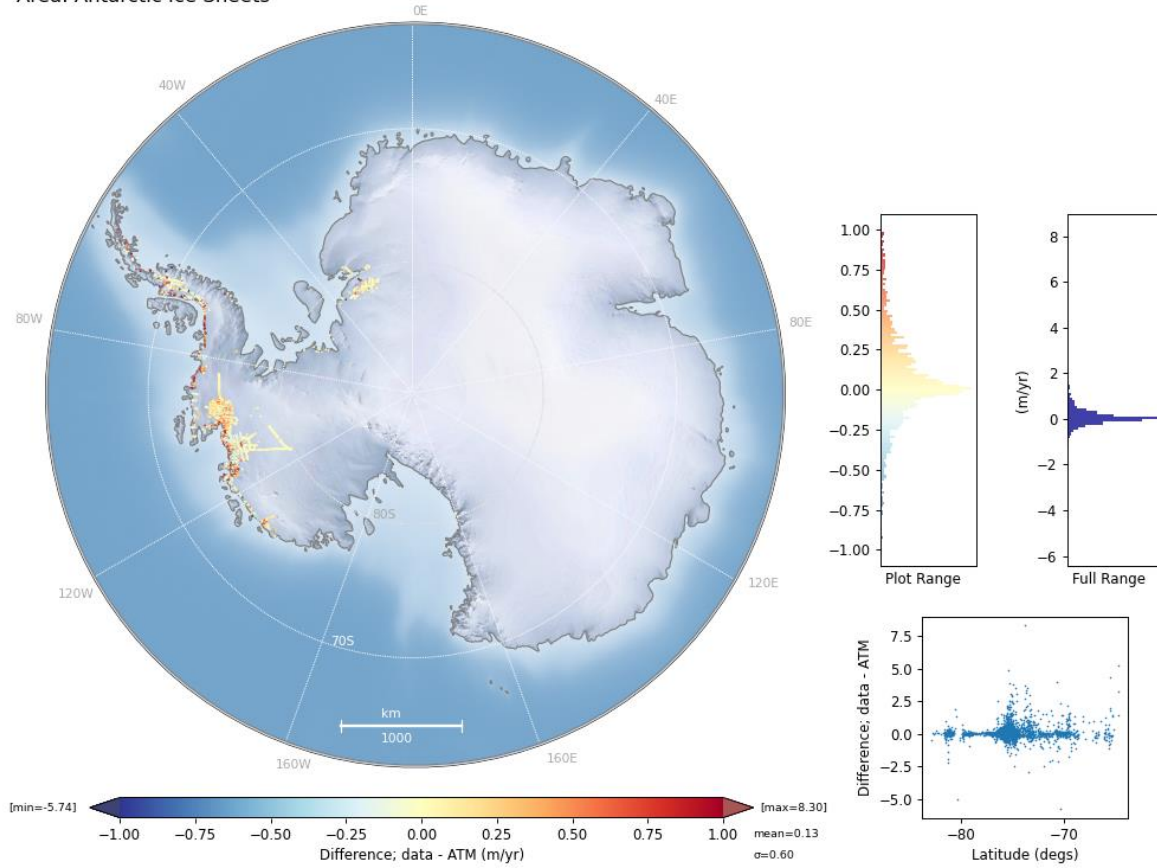
Figure 2-2: Comparison of CCI SEC and ASIRAS surface elevation change rates, using all selected data.

The results of the whole-region comparison are shown as a histogram and scatter plot in Figure 2-3 below.
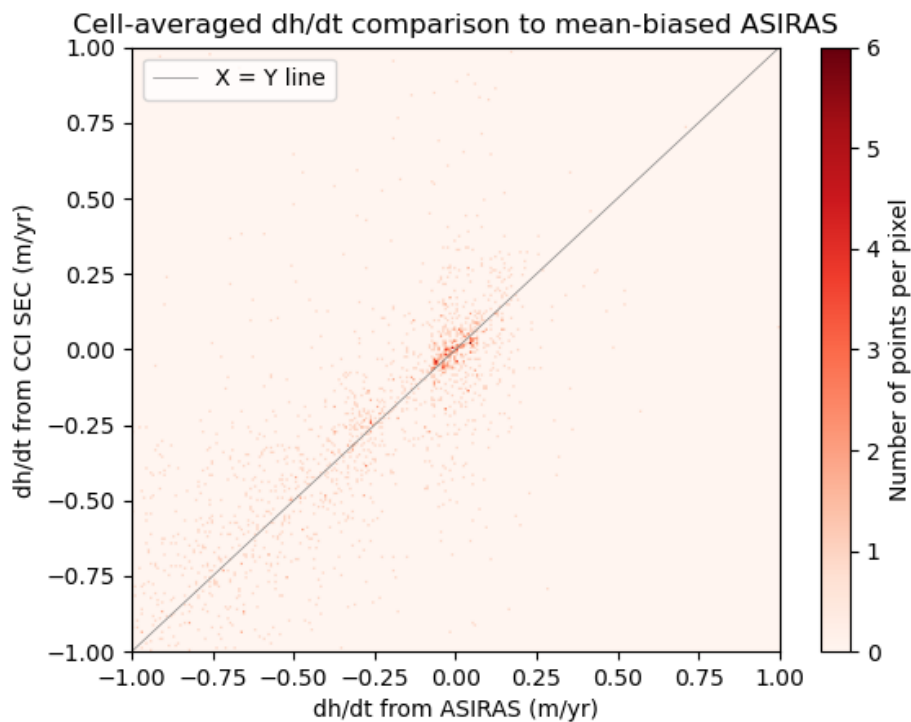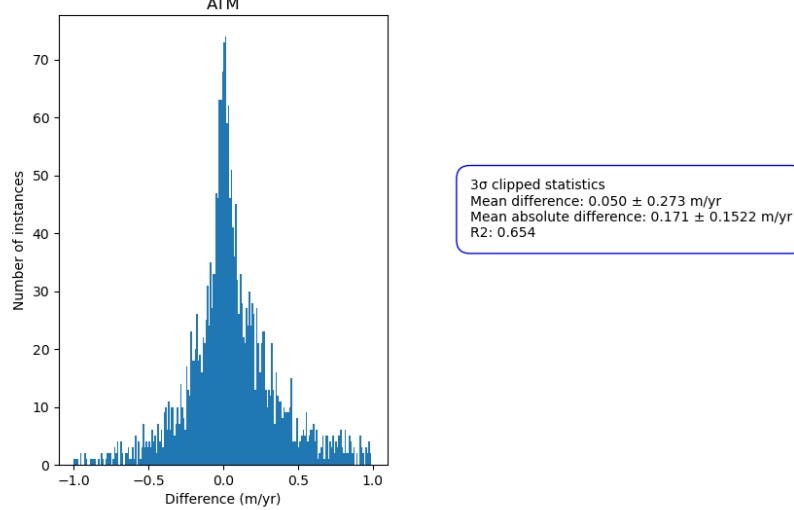
Figure 2-3: Histogram (above) and scatter plot (below) showing the distribution of differences between the satellite surface elevation change from the CCI SEC product, and the ASIRAS surface elevation change.

Statistics on the difference in change, CCI SEC minus ASIRAS, are compiled. Comparison statistics are calculated from a restricted dataset which excludes outliers by only

considering data points within ±3 standard deviations from the mean of the whole, original dataset.

The statistics for the dataset as a whole are:

- Absolute mean difference: 0.17 m/yr

- Absolute standard deviation of difference: 0.15 m/yr

- Coefficient of determination, R2: 0.65

- Mean slope of cells considered: 0.89°

- Number of cells considered: 2519

- Number of datapoints in total considered: 252368

Statistics on the difference in change, CCI SEC minus ASIRAS, for each basin considered separately are tabulated below. The number of cells used in each basin is noted as the SEC products were only compared when a result existed for both datasets. The mean slope of the cells used in each basin is also noted, as a measure of its terrain variability.

Table 2-1: Table, showing statistics of the difference between the CCI SEC and ASIRAS datasets for all validation basins. WA = West Antarctica, EA = East Antarctica, AP = Antarctic peninsula. Figures rounded to two decimal places.

	Absolute mean (m/yr)	Absolute standard deviation (m/yr)	R2, coefficient of determination	Number of cells considered	Basin mean slope (degrees)
WA, basin 1	0.03	0.03	0.03	28	0.36
EA, basin 2	0.13	0.16	0.87	6	0.96
EA, basin 3	0.08	0.08	0.00	226	0.50
WA, basin 19	0.02	0.01	0.54	35	0.08
WA, basin 20	0.26	0.19	0.64	198	1.33
WA, basin 21	0.16	0.14	0.71	745	0.70
WA, basin 22	0.20	0.16	0.76	719	0.53
WA, basin 23	0.30	0.25	0.31	116	1.28
AP, basin 24	0.25	0.26	0.11	254	1.55
AP, basin 25	0.34	0.32	0.19	72	1.77

AP, basin 26	0.38	0.40	0.00	84	2.16
AP, basin 27	0.08	0.07	0.02	36	1.15

Histograms of the separate basin comparisons are shown in **Figure 2-4** below.
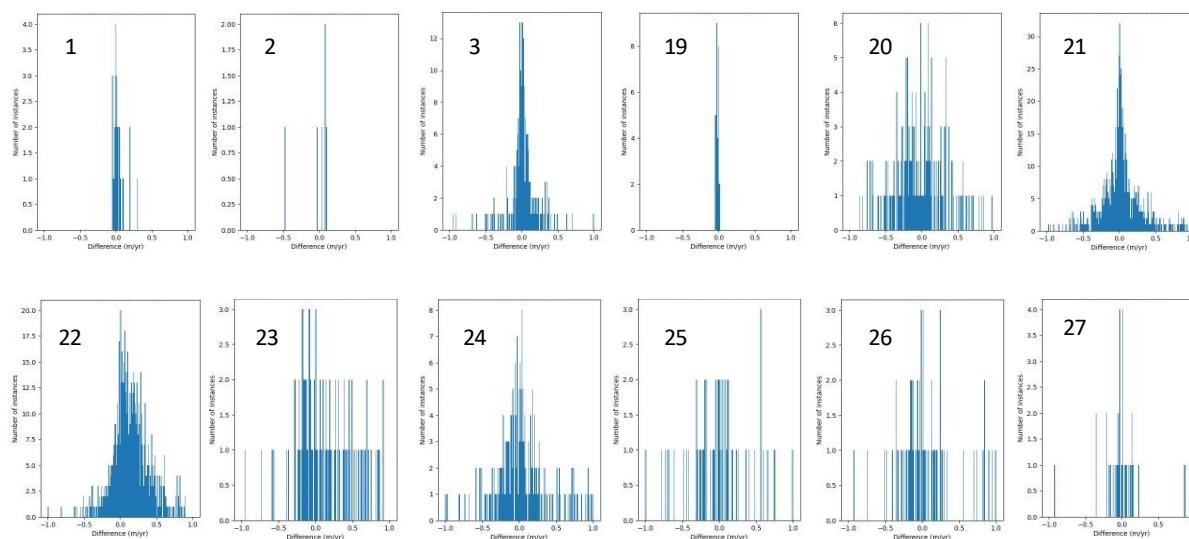
Figure 2-4: Histograms of CCI SEC and ASIRAS surface elevation change differences, for separate basins (basin number top left in each case).

In summary these results show that the mean difference between the validation dataset and the SEC product is less than 0.4 metres per year in all areas, although the correlation between signals is poor in the poorly sampled and highly sloping basins, with the lowest of the well-correlated differences generally occurring in West Antarctica. We attribute the larger difference between the validation data and the SEC product on the Antarctic Peninsula, in comparison to West Antarctica, to the more steeply sloping topography which is known to be more challenging terrain for the altimeter data retrieval to operate in.

2.4 Acknowledgement of the data contributor for SEC validation

The following dataset was used for the present validation:

Studinger, M. S. 2014, updated 2016. IceBridge ATM L4 Surface Elevation rate of Change, Version 1, Antarctica subset. Boulder, Colorado, USA. NASA National Snow and Ice Data Center Distributed Active Archive Centre. Doi:http://dx.doi.org/10.5067/BCW6CI3TXOCY. Accessed 25th May 2017.

3 Ice Velocity (IV)

This chapter describes the activities carried out to assess the quality of the IV products generated within AIS CCI+. The intercomparison and validation activities reported here concern specifically the monthly Antarctic IV mosaics derived by Sentinel-1 (S1) SAR data acquired from Jan 2017 till Aug 2020 (Figure 3-1). The activities supplement the previous validation efforts for IV, that were caried out within AIS CCI (Phase 1 and phase 2). These included intercomparisons of the multi-annual Antarctic IV mosaic as well as single S1 image pairs with in-situ GPS data, published velocity datasets and data derived from other sensors. Additionally quality assessment (QA) tests were performed such as the analysis of the IV in stable terrain. The results of these tests are described in [RD2]. In Antarctic Ice Sheet CCI+ detailed algorithm intercomparisons between project partners were carried out focusing on the tidal and pressure correction for floating ice. The results of these intercomparisons are described in the annex to [RD3]. Here we extent the QA efforts for the newly generated datasets including the stable terrain test and intercomparisons with an external ice velocity map.
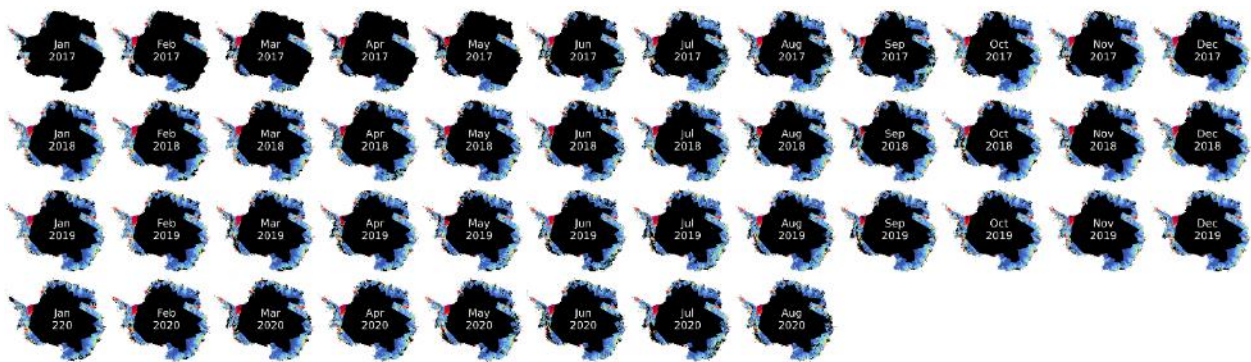

Figure 3-1: Monthly IV mosaics of the Antarctic coastal margin for the period January 2017 till August 2020 derived from Copernicus Sentinel-1.

3.1 Validation data

Due to sparsity of in-situ GPS data acquired in the period of the products generated within Antarctic Ice Sheet CCI+ (2017-2020) the validation and QA activities are restricted to intercomparisons with ice velocity maps for overlapping periods and the stable terrain test.

External Ice Velocity Map: As part of the NASA Making Earth System Data Records for Use in Research Environments (MEaSUREs) Program annual Antarctic IV maps were assembled derived from multi-sensor SAR data and optical imagery acquired between 2005 and 2017 (Mouginot et al., 2017a). The maps combine data derived from the Japanese Space Agency's (JAXA) ALOS PALSAR, the European Space Agency's (ESA) ENVISAT ASAR and Copernicus Sentinel-1, the Canadian Space Agency's (CSA) RADARSAT-1, RADARSAT-2 and the German Aerospace Agency's (DLR) TerraSAR-X (TSX) and TanDEM –X (TDX), and are integrated with optical imagery from the U.S.

Geological Survey's (USGS) Landsat-8. Data are available in NetCDF format through NSIDC at 1 km spatial resolution (Data Set ID: NSIDC-0720; Mouginot et al., 2017b).

Rock Outcrop Map: For the stable terrain test we use a rock outline shapefile derived from Landsat-8 Operational Land Imager (OLI) images (Figure 3-2; Burton-Johnson et al., 2016). The dataset is generated using a new and automated methodology for snow and rock differentiation that excludes areas of snow (both illuminated and shaded), clouds and liquid water whilst identifying both sunlit and shaded rock. The method achieves higher and more consistent accuracies than alternative data and methods such as the normalized difference snow index (NDSI). The images were acquired in austral summers between October 2013 and March 2015. The dataset is provided as a supplement with the paper (Burton-Johnson et al., 2016).
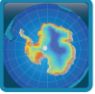
Figure 3-2: Map of Antarctica showing in blue floating ice shelves and in red the rock outcrop shapefile used for the stable terrain test (Burton-Johnson et al., 2016).

3.2 Validation procedure

For the quality assessment (QA) of IV products a series of standard tests/measures were developed providing various levels of validation [RD2]. Here we apply two of these:

1) The product is evaluated against publicly available products covering the same area. These generally cover a different time span, have a different resolution, and are assembled from different sensors. Nevertheless, they provide a level of quality assurance, in particular in areas where little change is to be expected. Here, we use the multi-sensor annual map running from July 2016 till July 2017 (Mouginot et al., 2017b), for intercomparison with the 6 monthly maps for January till July 2017. For the

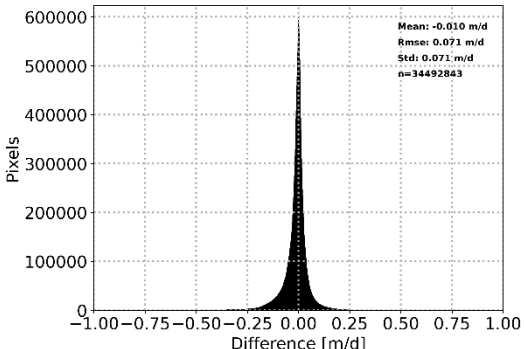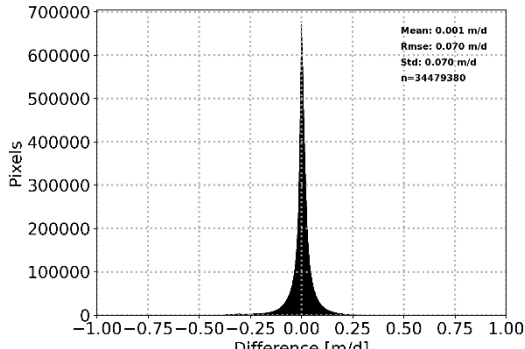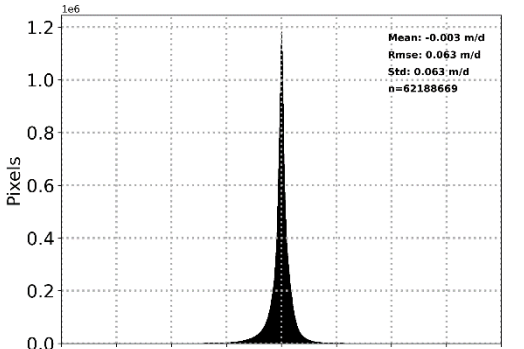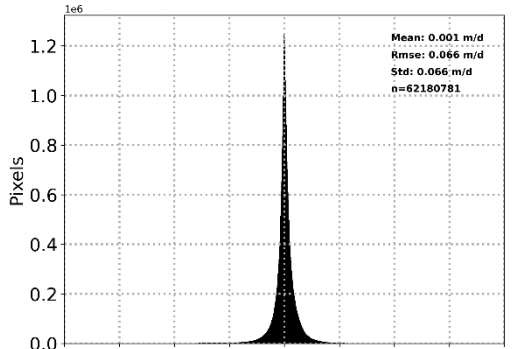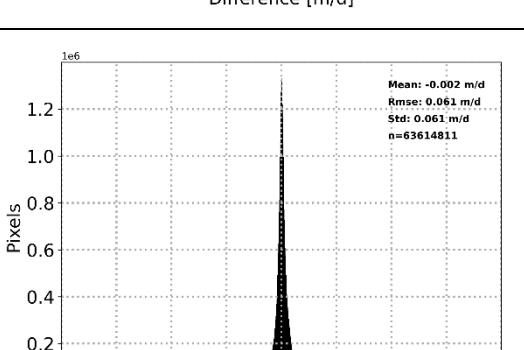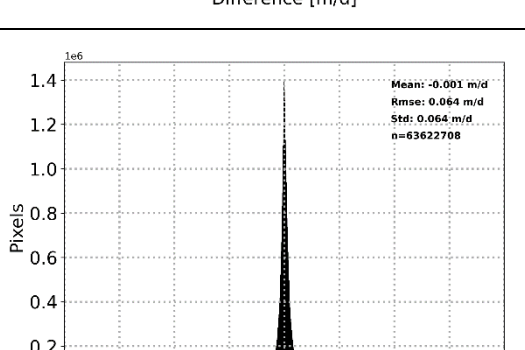intercomparison we resample the validation dataset to the same grid spacing, projection and extent. Only overlapping areas are used for the pixel-by-pixel intercomparison. And differences larger than 1 m/day are excluded for the calculation of statistics. The quality metrics that are calculated are: Mean and RMSE of the difference of velocity components (E,N).

2) The product is evaluated through the analysis of velocity measured on stable terrain where no motion is expected. This gives a good overall indication for the bias introduced by the end-to-end velocity retrieval including co-registration of images, velocity retrieval, etc. The results for the ice covered (moving) terrain are separated from ice-free (stable) terrain using a polygon of the rock outlines (Burton-Johnson et al., 2016). Buffers around the polygons are applied before extraction of the stable ground for statistics calculation, or alternatively a final visual check for misclassified stable terrain will be performed in order to avoid potential errors introduced by the area polygon. The stable terrain test is performed for all the generated monthly maps (Jan 2017-Aug 2020), assuming no change in the ice-free areas. The quality metrics of the test provides: Mean and RMSD of the velocity over stable terrain; mean values should be close to 0.

3.3 Validation outcome

We present difference histograms and maps for both the easting and northing components (Figure 3-3) including statistics (Table 3-1) for the period providing an overlap between the two datasets: Jan-Jun 2017. The generated figures and statistics illustrate the performance and level of agreement between the IV datasets. For the intercomparison of the S1 IV maps and MEaSUREs the mean difference for all maps is 0.00 md^{-1} (RSME: 0.06 m d^{-1}) for both the easting and northing components indicating an excellent agreement. Larger deviations are concentrated in a few regions (for example Pine Island Glacier and Stancomb-Wills Ice Tongue) likely reflect actual change or might be related to different window sizes leading to differences in for example shear margins of fast glaciers.

Month	Easting	Nothing
Jan		
Feb		
Mar		

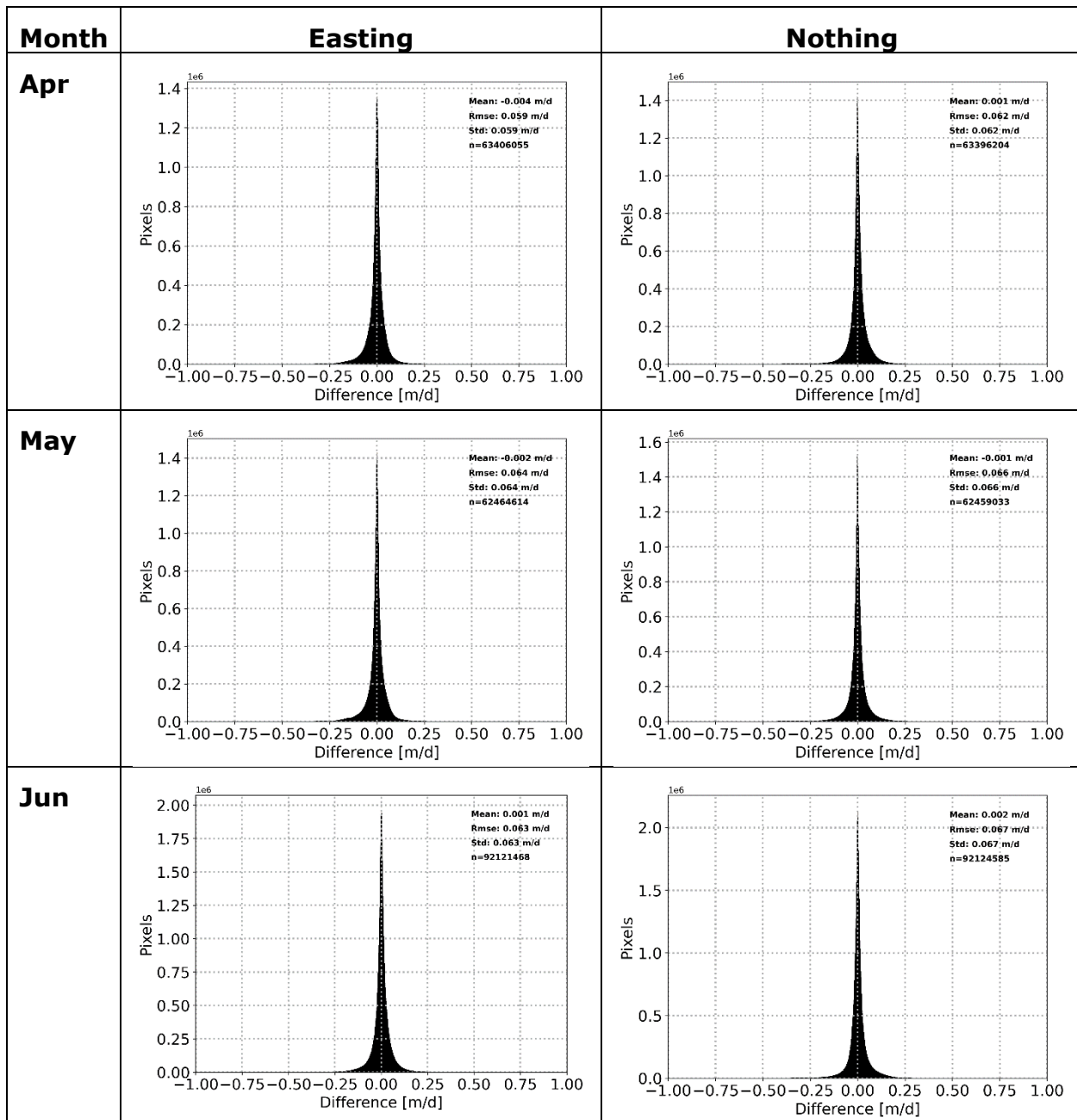| Month	Easting	Nothing
Apr		
May		
Jun		

Figure 3-3: Difference histograms for easting (left) and northing (right) component for the intercomparison between the ENVEO Sentinel-1 ice sheet monthly velocity map (Jan 2017-Jun 2017) and the MEaSUREs annual velocity map 2016/17 (Mouginot et al., 2017b).

Table 3-1: Summary of IV comparison quality assessment.

Product Analysed	Reference dataset Measures	Number of pixels used in analysis	Mean difference Easting [m d-1]	RMSE difference Easting [m d-1]	Mean difference Northing [m d-1]	RMSE difference Northing [m d-1]
20170101-ESACCI-L3C-AIS-IV-S1-1M_200m-fv1.0.nc	Antarctica_ice_velocity_2016_2017_1km_v1.nc	~34.5 M	-0.01	0.07	0.00	0.07
20170201-ESACCI-L3C-AIS-IV-S1-1M_200m-fv1.0.nc	Antarctica_ice_velocity_2016_2017_1km_v1.nc	~62.2 M	0.00	0.06	0.00	0.07
20170301-ESACCI-L3C-AIS-IV-S1-1M_200m-fv1.0.nc	Antarctica_ice_velocity_2016_2017_1km_v1.nc	~63.6 M	0.00	0.06	0.00	0.06
20170401-ESACCI-L3C-AIS-IV-S1-1M_200m-fv1.0.nc	Antarctica_ice_velocity_2016_2017_1km_v1.nc	~63.4 M	0.00	0.06	0.00	0.06
20170501-ESACCI-L3C-AIS-IV-S1-1M_200m-fv1.0.nc	Antarctica_ice_velocity_2016_2017_1km_v1.nc	~62.5 M	0.00	0.06	0.00	0.07
20170601-ESACCI-L3C-AIS-IV-S1-1M_200m-fv1.0.nc	Measures Antarctica_ice_velocity_2016_2017_1km_v1.nc	~92.1 M	0.00	0.06	0.00	0.07

The stable ground test is carried out for all IV products. The red areas depicted in Figure 3-2 show the stable regions for which the analysis is performed. Example histograms are presented in Figure 3-4 illustrating the distribution of the easting and northing velocity components for January 2020. Ideally these should be centered at zero for stable areas. Deviations can be due to several causes including errors in the rock shapefile, errors in the layover mask and artifacts produced by the algorithm. The outcome of the stable ground test are summarized in Table 3-2. Results indicate a mean of 1.8 cm d^{-1} in easting and 0.7 cm d^{-1} in northing direction, with a mean RMSE of 0.190 m d^{-1} for the easting and 0.178 m d^{-1} for the northing velocity component respectively.
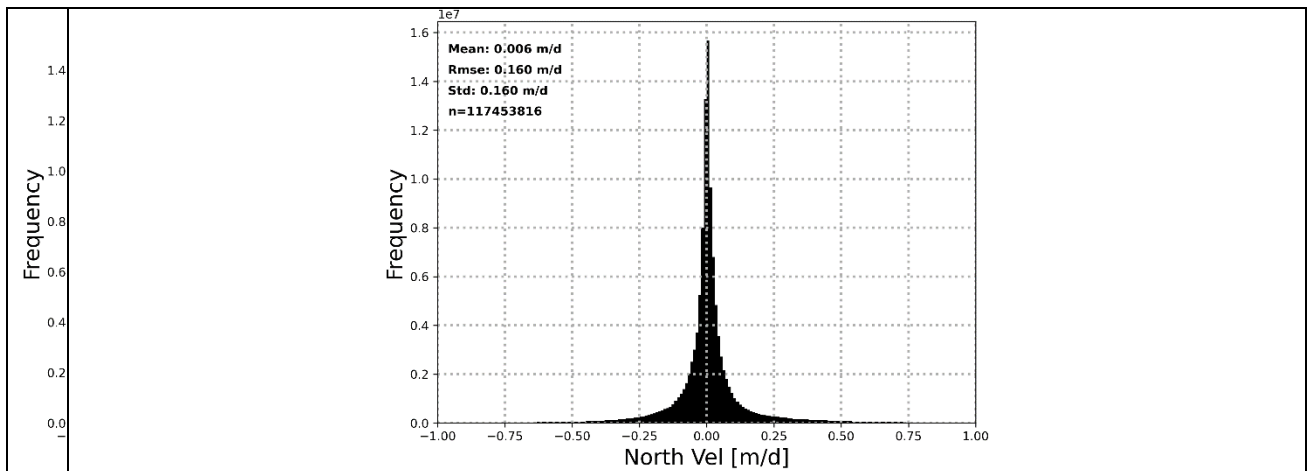
Figure 3-4: Histogram of easting (left) and northing (right) velocity on stable terrain for January 2020.

Table 3-2: Summary of stable rock quality assessment for averaged S1 ice velocity map (Jan 2017-Aug 2020).

Product Analysed	Mean E [m d^{-1}]	RMSE E [m d^{-1}]	Mean N [m d^{-1}]	RMSE N [m d^{-1}]
20170101-ESACCI-L3C-AIS-IV-S1-1M_200m-fv1.0.nc	-0.014	0.245	0.039	0.202
20170201-ESACCI-L3C-AIS-IV-S1-1M_200m-fv1.0.nc	-0.002	0.208	0.012	0.190
20170301-ESACCI-L3C-AIS-IV-S1-1M_200m-fv1.0.nc	0.001	0.201	0.006	0.189
20170401-ESACCI-L3C-AIS-IV-S1-1M_200m-fv1.0.nc	-0.007	0.207	0.004	0.192
20170501-ESACCI-L3C-AIS-IV-S1-1M_200m-fv1.0.nc	-0.004	0.208	0.001	0.197
20170601-ESACCI-L3C-AIS-IV-S1-1M_200m-fv1.0.nc	0.027	0.193	0.004	0.180
20170701-ESACCI-L3C-AIS-IV-S1-1M_200m-fv1.0.nc	0.024	0.193	0.009	0.181
20170801-ESACCI-L3C-AIS-IV-S1-1M_200m-fv1.0.nc	0.021	0.194	0.007	0.181
20170901-ESACCI-L3C-AIS-IV-S1-1M_200m-fv1.0.nc	0.019	0.200	0.006	0.184
20171001-ESACCI-L3C-AIS-IV-S1-1M_200m-fv1.0.nc	0.024	0.189	-0.001	0.173
20171101-ESACCI-L3C-AIS-IV-S1-1M_200m-fv1.0.nc	0.025	0.184	0.001	0.175
20171201-ESACCI-L3C-AIS-IV-S1-1M_200m-fv1.0.nc	0.017	0.189	0.002	0.175
20180101-ESACCI-L3C-AIS-IV-S1-1M_200m-fv1.0.nc	0.014	0.182	0.002	0.172

20180201-ESACCI-L3C-AIS-IV-S1-1M_200m-fv1.0.nc	0.012	0.185	0.007	0.171
20180301-ESACCI-L3C-AIS-IV-S1-1M_200m-fv1.0.nc	0.017	0.183	0.001	0.165
20180401-ESACCI-L3C-AIS-IV-S1-1M_200m-fv1.0.nc	0.016	0.183	0.004	0.171
20180501-ESACCI-L3C-AIS-IV-S1-1M_200m-fv1.0.nc	0.020	0.188	0.003	0.174
20180601-ESACCI-L3C-AIS-IV-S1-1M_200m-fv1.0.nc	0.022	0.194	0.002	0.182
20180701-ESACCI-L3C-AIS-IV-S1-1M_200m-fv1.0.nc	0.024	0.195	0.006	0.178
20180801-ESACCI-L3C-AIS-IV-S1-1M_200m-fv1.0.nc	0.023	0.197	0.004	0.183
20180901-ESACCI-L3C-AIS-IV-S1-1M_200m-fv1.0.nc	0.026	0.193	0.002	0.181
20181001-ESACCI-L3C-AIS-IV-S1-1M_200m-fv1.0.nc	0.027	0.187	0.006	0.178
20181101-ESACCI-L3C-AIS-IV-S1-1M_200m-fv1.0.nc	0.020	0.190	0.001	0.178
20181201-ESACCI-L3C-AIS-IV-S1-1M_200m-fv1.0.nc	0.018	0.185	0.002	0.172
20190101-ESACCI-L3C-AIS-IV-S1-1M_200m-fv1.0.nc	0.015	0.184	0.004	0.171
20190201-ESACCI-L3C-AIS-IV-S1-1M_200m-fv1.0.nc	0.013	0.182	0.011	0.168
20190301-ESACCI-L3C-AIS-IV-S1-1M_200m-fv1.0.nc	0.022	0.178	0.011	0.172
20190401-ESACCI-L3C-AIS-IV-S1-1M_200m-fv1.0.nc	0.020	0.180	0.007	0.170
20190501-ESACCI-L3C-AIS-IV-S1-1M_200m-fv1.0.nc	0.022	0.189	0.008	0.173
20190601-ESACCI-L3C-AIS-IV-S1-1M_200m-fv1.0.nc	0.023	0.186	0.016	0.179
20190701-ESACCI-L3C-AIS-IV-S1-1M_200m-fv1.0.nc	0.029	0.189	0.012	0.179
20190801-ESACCI-L3C-AIS-IV-S1-1M_200m-fv1.0.nc	0.023	0.191	0.011	0.184
20190901-ESACCI-L3C-AIS-IV-S1-1M_200m-fv1.0.nc	0.029	0.186	0.009	0.182
20191001-ESACCI-L3C-AIS-IV-S1-1M_200m-fv1.0.nc	0.022	0.187	0.006	0.178
20191101-ESACCI-L3C-AIS-IV-S1-1M_200m-fv1.0.nc	0.020	0.188	0.005	0.175
20191201-ESACCI-L3C-AIS-IV-S1-1M_200m-fv1.0.nc	0.021	0.182	0.007	0.171
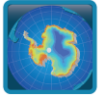
20200101-ESACCI-L3C-AIS-IV-S1-1M_200m-fv1.0.nc	0.012	0.175	0.006	0.160
20200201-ESACCI-L3C-AIS-IV-S1-1M_200m-fv1.0.nc	0.020	0.178	0.009	0.168
20200301-ESACCI-L3C-AIS-IV-S1-1M_200m-fv1.0.nc	0.020	0.177	0.006	0.170
20200401-ESACCI-L3C-AIS-IV-S1-1M_200m-fv1.0.nc	0.017	0.183	0.008	0.171
20200501-ESACCI-L3C-AIS-IV-S1-1M_200m-fv1.0.nc	0.023	0.184	0.011	0.176
20200601-ESACCI-L3C-AIS-IV-S1-1M_200m-fv1.0.nc	0.029	0.186	0.010	0.183
20200701-ESACCI-L3C-AIS-IV-S1-1M_200m-fv1.0.nc	0.033	0.187	0.017	0.183
20200801-ESACCI-L3C-AIS-IV-S1-1M_200m-fv1.0.nc	0.021	0.194	0.010	0.184
MEAN	**0.018**	**0.190**	**0.007**	**0.178**

4 Grounding Line Location (GLL)

This chapter gives an update of the activities carried out to assess the quality of the GLL products.

4.1 Independent validation data

4.1.1 Requirements

The boundary of the grounded ice sheet includes a variety of structural conditions:

- glacier tongues (ice thickness gradually decreases)

- ice cliffs (ice breaks off and falls onto the ground or sea ice)

- ice shelves (ice flows into the ocean and remains attached to the grounded ice until it calves). This is the dominant situation in Antarctica, stretching about 19,000 km in length (British Antarctic Survey, 2005).

For the most cases, e.g. an outlet glacier with a floating tongue or on an ice shelf, the GLL is not directly observable. Therefore, the validation of the GLL outcome is the same as in the AIS_cci project phase 2015 – 2018 when it was carried out against similar products consisting of indirectly derived GLLs from a variety of satellite data and the appropriate indirect method.

Although within AIS_cci we do not aim at deriving the GLL on a continental scale we selected the most commonly used Antarctica-wide GLL databases available for download at NSIDC for validation. A detailed description is given in Section 4.1.2.
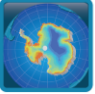
In order to facilitate the intercomparison of the various GLLs, the AIS_cci GLL product is annotated with time stamps and ocean tide level differences. Since this information is not given for the validation datasets an interpretation of the comparison must be done with care in particular with respect to GLL migration. Therefore, we limit our comparison to a purely geometrical/spatial approach which does not take ocean tide changes into account. Only the comparison with interferometric GLLs derived from same SAR data have a reduced tidal effect.

4.1.2 Sources

Three comprehensive data sets were used to validate the AIS_cci GLL. Their details are given below.

(1) The Antarctic grounding line derived from the MODIS Mosaic of Antarctica (**MOA**) from (Scambos et al., 2007)

This GLL was generated together with the coastline from the digital image mosaic of surface morphology assembled from 260 Moderate-resolution Imaging Spectroradiometer (MODIS) images acquired between Nov. 2003 and Feb. 2004. The good geolocation and slope sensitivity of the MOA surface morphology image made a continent-wide mapping of the coastline and the grounding line possible. In (Scambos et al., 2007) the grounding line is defined as the coastal slope break between floating

and grounded ice (I_b in Figure). The GLL was manually digitized by following the seaward-most continuous slope break on the surface inside of (or equal to) the permanent coastline in images of the MOA surface morphology dataset.

The coastline and the grounding line are two vector files which can be downloaded at ftp://sidads.colorado.edu/pub/DATASETS/nsidc0280_moa2004/coastlines/ in various formats. The spatial resolution is 250 m. The location precision is estimated to be no worse than ±250 m. The MOA grounding line is the only available dataset which has a 100% complete coverage including continent and islands. The time stamp (date/time) of the MODIS acquisitions used to generate the MOA grounding line segments is unfortunately not given.
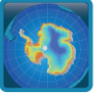
(2) The Antarctic Surface Accumulation and Ice Discharge (**ASAID**) IPY project, from (Bindschadler et al., 2011)

Two ice-dynamic features were mapped within this project: the seaward boundary of surface morphology associated with grounded ice (I_b in Figure) and the landward boundary of freely floating ice shelves or hydrostatic line (H in Figure). The boundaries were generated at a spatial resolution of 15 m from Landsat-7 imagery acquired between 1999 and 2003 and ICESat/GLAS laser altimetry from two observation periods in 2003 and 2008. The photoclinometry procedure is based on the relationship between the pixel brightness in the optical image and the surface slope. In addition an ICESat/GLAS elevation (up-sun and down-sun) is required in order to delimitate the subimage where the brightness-slope relationship is applied. The authors mention that identifying where the fast-moving glaciers discharge into ice shelves was the most challenging task. In these cases, additional MOA imagery is analysed and at all locations where the MODIS shows additional grounded ice features it will be compared to Landsat. Here the ASAID GLL follows the MOA GLL.

The grounding line and hydrostatic line locations can be downloaded at http://nsidc.org/data/docs/agdc/nsidc0489_bindschadler/. The spatial resolution is 15 m. The positional accuracies of the ASAID GLL vary from ±52 m for the land and open ocean terminating segments to ±502 m for the outlet glaciers. The hydrostatic line (H) is positioned with errors of over 2 km. The ASAID GLL is consistent around the continent, but covers only 3 islands. The time stamp (date/time) of the Landsat-7 acquisitions used to generate the ASAID GLL segments is not given.

(3) The **MEaSUREs** InSAR grounding lines from (Rignot et al., 2011b)

This GLL product consists of the mapped upper limit of tidal flexure (F in Figure) observed in differential interferograms (DInSAR) around Antarctica. The satellite data used initially are ERS-1/2 from 1992, 1994 and 1996, RSat-1 from 2000, RSat-2 from 2009 and ALOS PALSAR from 2007-2008 extending over a large time span for more than 15 years. Meanwhile the MEaSUREs product has been completed with new GLLs derived from recent Sentinel-1 and COSMO SkyMed data. The DInSAR technique to obtain the

distinct signature of elastic bending is the same as that used in the present AIS_cci project. The GLL was manually mapped in the SAR geometry and georeferenced afterwards.

The grounding line can be downloaded at https://nsidc.org/data/nsidc-0498 in the currently available Version 2.0 (Rignot et al., 2017). The spatial resolution is 50 m. The standard deviation of the errors is ±100 m and was found from comparison with multiple mappings, instruments, and epochs (including the MOA grounding line). Locally greater variations are observed. In some cases, km-wide migrations were detected.

The coverage is incomplete in some areas (due to the lack of coherence) while in other areas multiple inner flexure lines (F) were obtained at different dates. As time stamp only the date of the SAR acquisitions used to generate the MEaSUREs GLL segments, and the satellite orbit are annotated in the product which makes the extraction of ocean tide levels needed for comparison very laborious. Although an update of the MEaSUREs GLL product annotated with exact date/time stamps is expected this did not occur at this date and this limits the possibilities to extend the ocean tide level dependent validation to other areas.

> (4) The Machine Learning delineated GLL from Sentinel-1 A/B data of 2018 from (Mohajerani et al., 2021)

According to the authors this represents a complete grounding line delineation around the Antarctic Ice Sheet in the year 2018. The SAR data used are Sentinel-1 A/B with 6 and 12 days repeat pass. Besides the timely limited dataset, the difference to the MEaSUREs GLL is the automatic delineation of the grounding line from the double difference interferograms which is carried out through machine learning. The product consists of multitemporal GLL segments with large spatial spread and in some areas looking unrealistic. Moreover, this product – similar to the MEASUREs GLL - has no annotation in the attribute table of the exact time stamp of the Sentinel-1 acquisitions. Therefore, we do not consider this data set appropriate to be used for the validation of the AIS_cci GLL products.
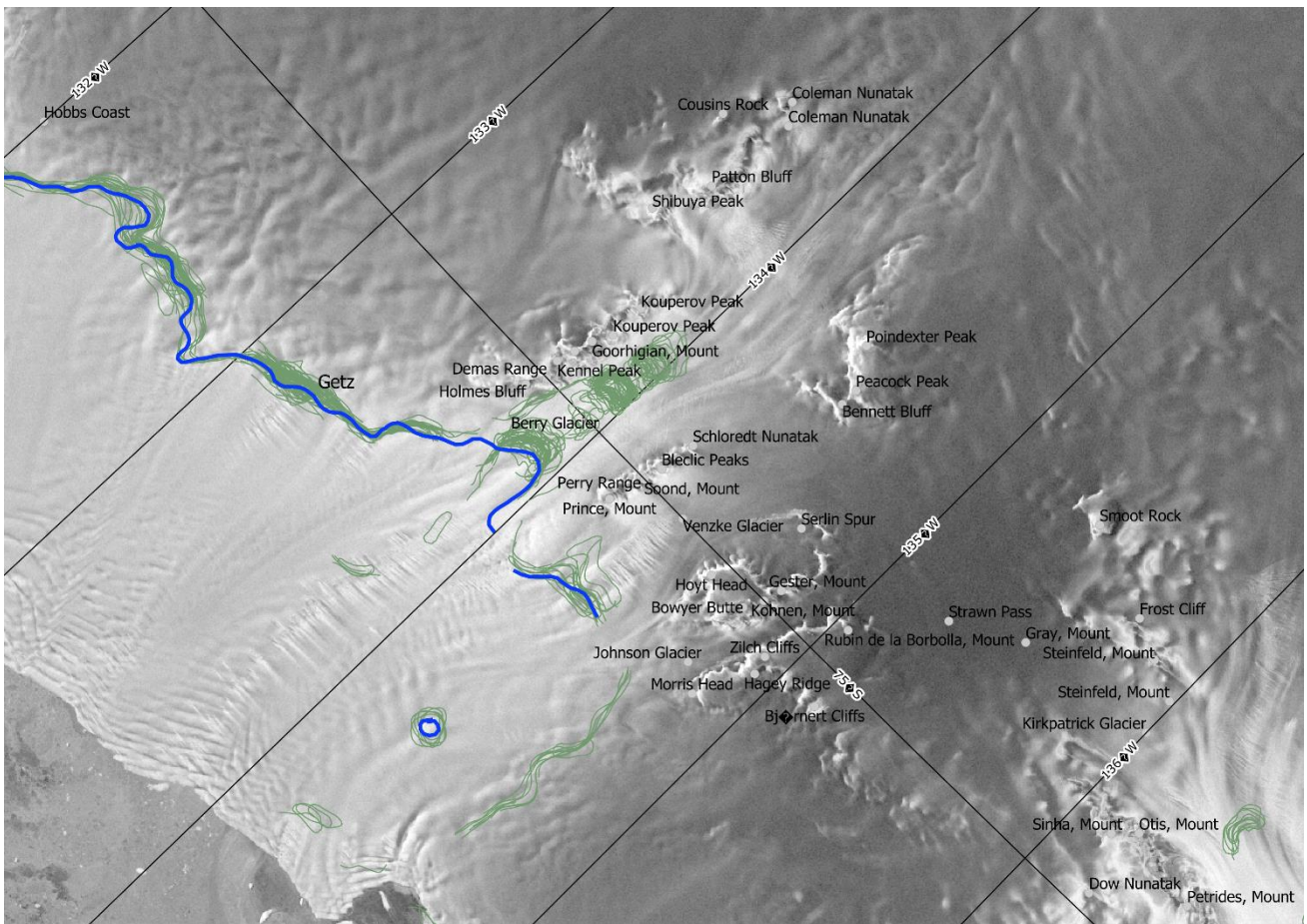
Figure 4-1: The AIS_cci GLL (blue line) and the time series of machine learning delineated GLLs (green lines) in the Getz area.

4.1.3 Assessment

Although the term "grounding line" is generally used to define the boundary of the grounded ice sheet and a floating ice shelf it can be applied to various datasets using different methodologies sensitive to different topographic or dynamic features. In order to avoid confusion when the different grounding line products are compared with the AIS_cci GLL the processes and features at the margin of the ice sheet are schematically outlined in Figure and will be discussed in the following.
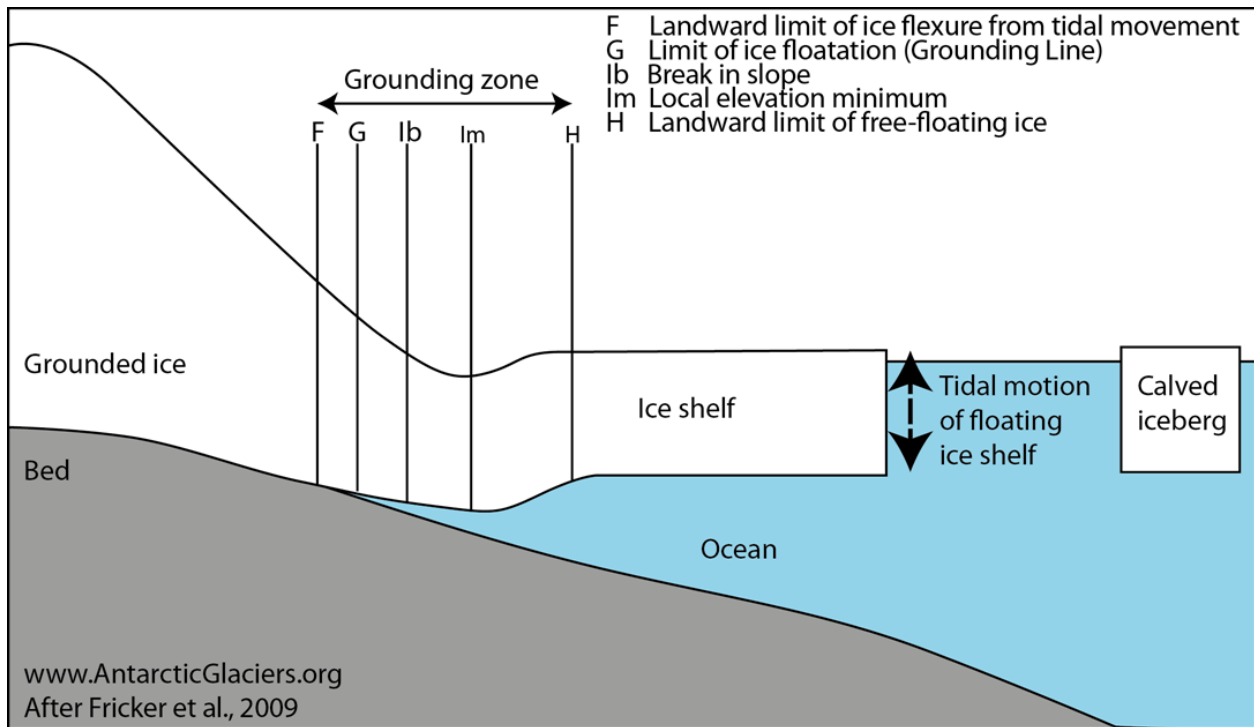
Figure 4-2: Processes and features at the grounding zone.

The grounding zone extends between the point F, the most seaward point not vertically displaced by tidal flexure, and H, the most landward location that experiences vertical motion equal to the magnitude of the ocean tide. G is the location where the ice losses contact to the bed (at low tide). I_b and I_m are inflections of the surface slope where the slope changes most rapidly (break in slope) and where the slope is zero, respectively. Different techniques determine different points within the grounding zone. H is not well known, but F and I_b have been extensively mapped.

The MOA and ASAID grounded ice boundaries (GLLs products) are most consistent with point I_b, the slope break. SAR sensors detect the band of flexure between F and H which appears as a typical pattern of dense fringes in the double difference interferograms. Although F is not identical with G, since F and G lay very close together (< 1 km) (Rignot et al., 2011b) the upper limit of flexure is treated as GLL. This is the case for MEaSUREs and AIS_cci (see RD4) products. Repeat laser altimetry can detect H and F from repeat-track analysis and I_b and I_m from single profiles (Bindschadler et al., 2011).

The zone F-H is typically 2-11 km wide on Antarctic glaciers but can also reach extreme values of up to 25 km in areas that are lightly grounded or where tidal flexure is highly contorted by boundary conditions. I_b is typically a few km downstream of G.

4.1.4 Selection

The AIS_cci grounding lines are validated against the independent datasets described in Section 4.1.2. The comparison is carried out on four areas (Figure 4-3). Additionally, the Schirmacher site has been divided into one area covered by Sentinel-1 and one area where ERS-1/2 data was used.
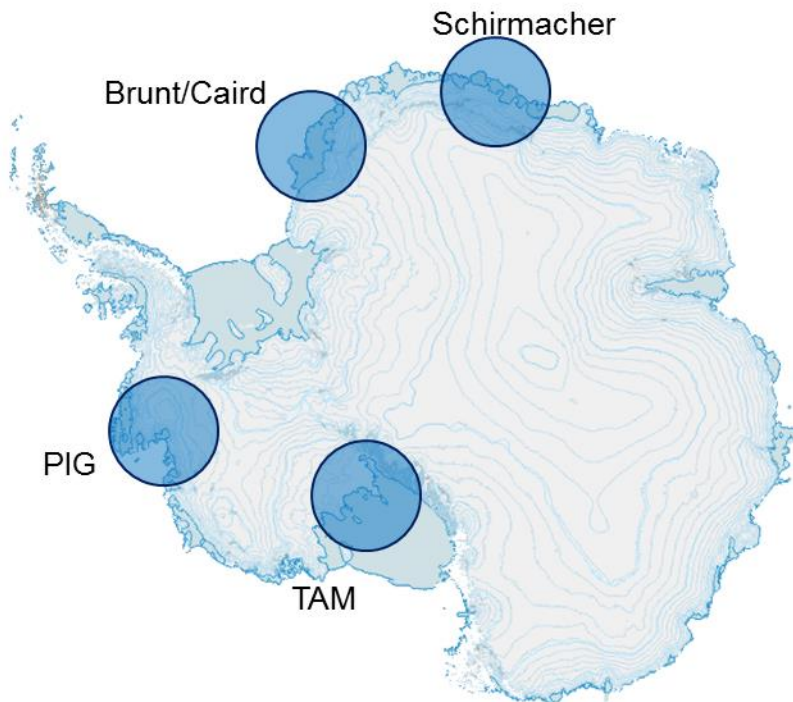

Figure 4-3: Validation test areas for the AIS_cci GLL products: Schirmacher, Brunt/Caird, PIG – Pine Island Glacier and TAM – Transantarctic Mountains.

4.2 Validation procedure

For the validation, the GLLs are compared with a spatial metric. A tide level dependent comparison is a goal for further comparisons later in the project but it is currently difficult to perform since no exact acquisition times are given in the other datasets. Using MEaSUREs date stamp and orbit number theoretically allows the determination of the actual acquisition time required for tide prediction. However, since this is a rather extensive task, it cannot be performed within the first year PVIR.

We carry out our analysis in four areas and compare AIS_cci GLLs with each of the GLLs described in the validation set (Section 4.1.2). If there is more than one GLL in a specific validation product all of them will be analyzed, since no temporal separation is currently performed.

The different GLL datasets are referenced as:

Reference	Description
AIS_cci	Our product derived from interferometric data
ASAID	ASAID GLL
MOA	MOA GLL
MEaSUREs	MEaSUREs GLL

All GLLs superimposed on the RSat-1 SAR backscattering mosaic are shown in Figure 4-4 to Figure 4-8. A first visual comparison suggests a good overall agreement between all GLL products within a range of 5 km to 10 km.
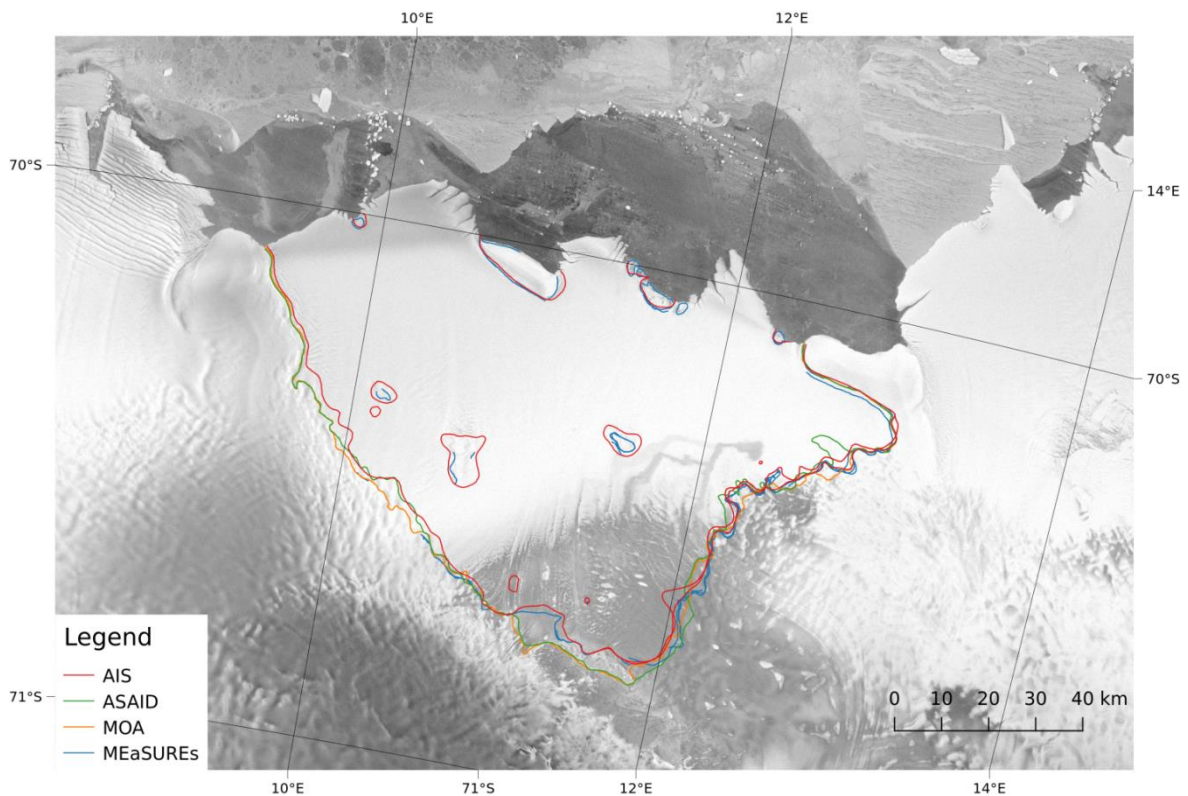
Figure 4-4: The Schirmacher ERS area (Nivlisen Ice Shelf) with all validation GLLs and the AIS GLL derived from ERS-1/2 data.

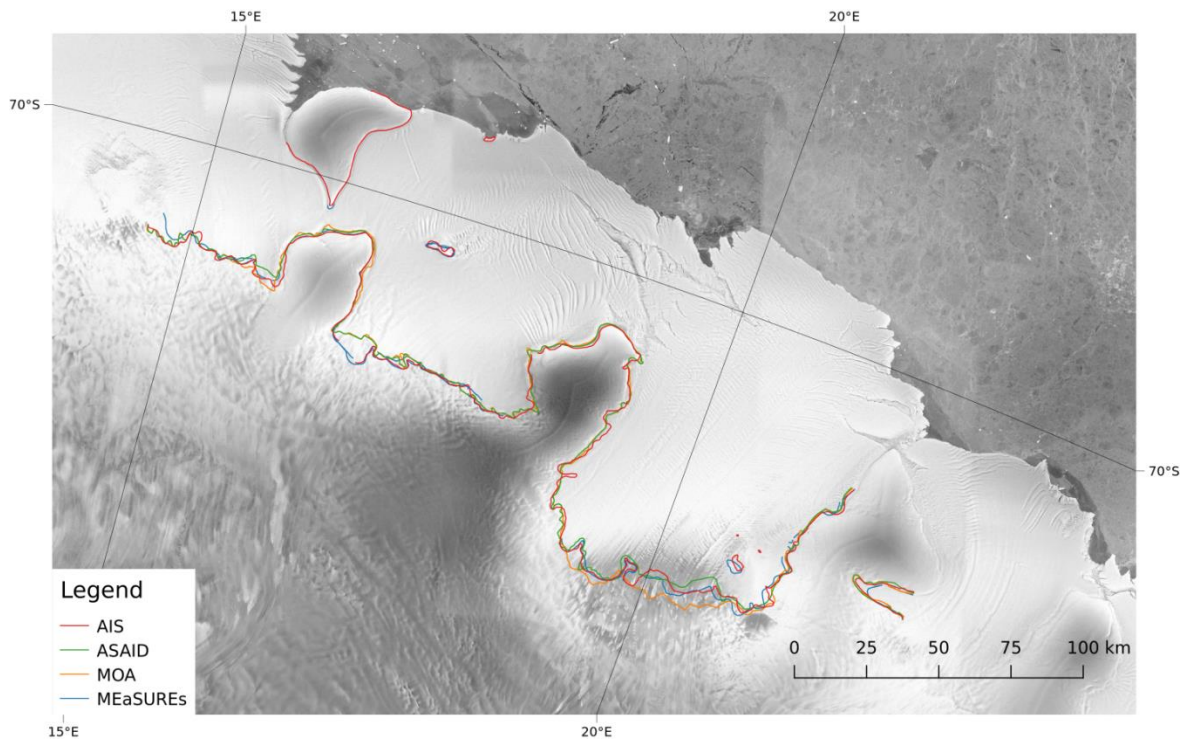**Figure 4-5:** The Schirmacher S1 area (Lazarevisen Ice Shelf) with all validation GLLs and the AIS_cci GLL derived from Sentinel-1 data.
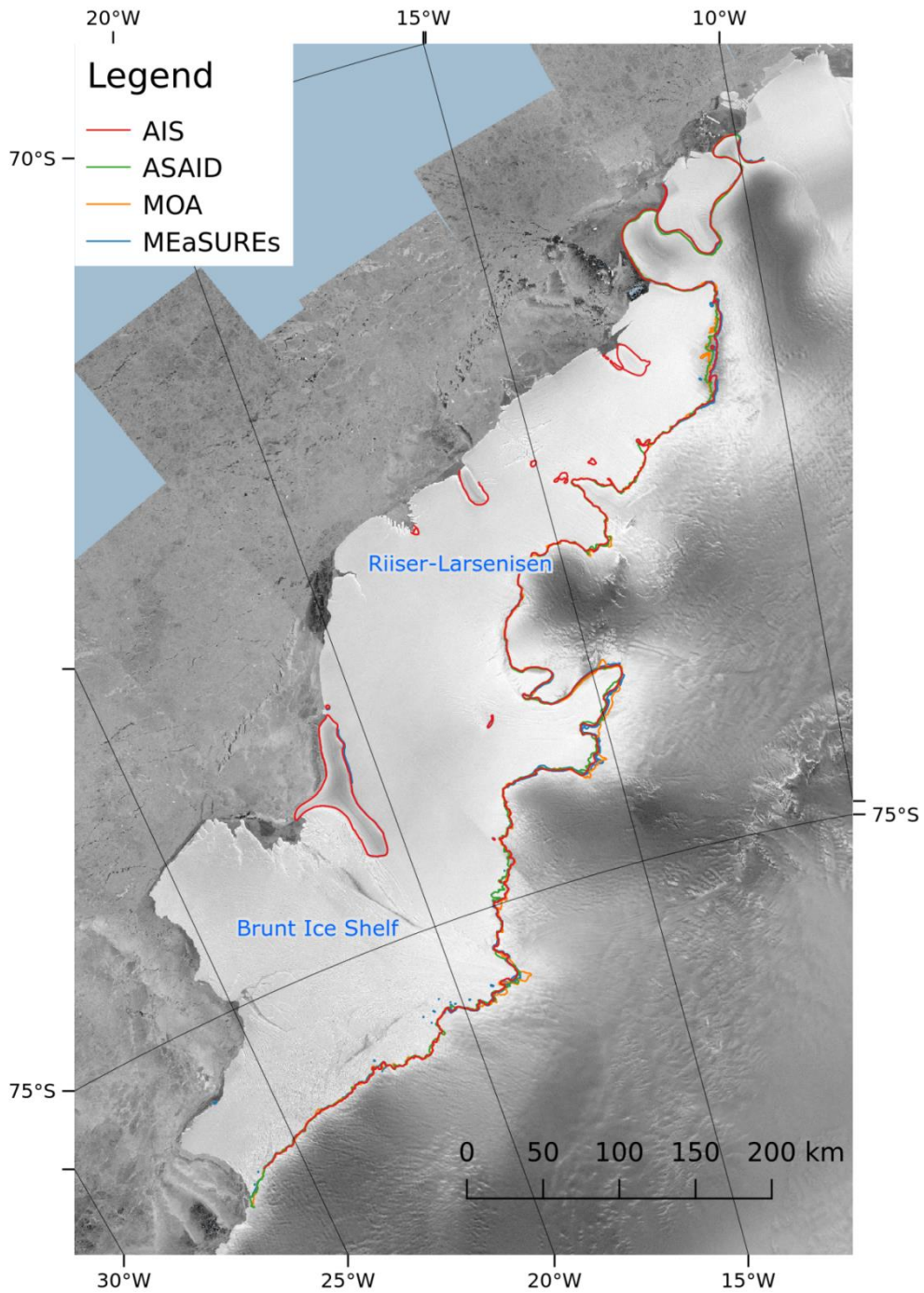
Figure 4-6: The Brunt Ice Shelf/Caird Coast area (incl. Riiser Larsenisen Ice Shelf) with all validation GLLs and the AIS_cci GLL derived from ERS-1/2 data.
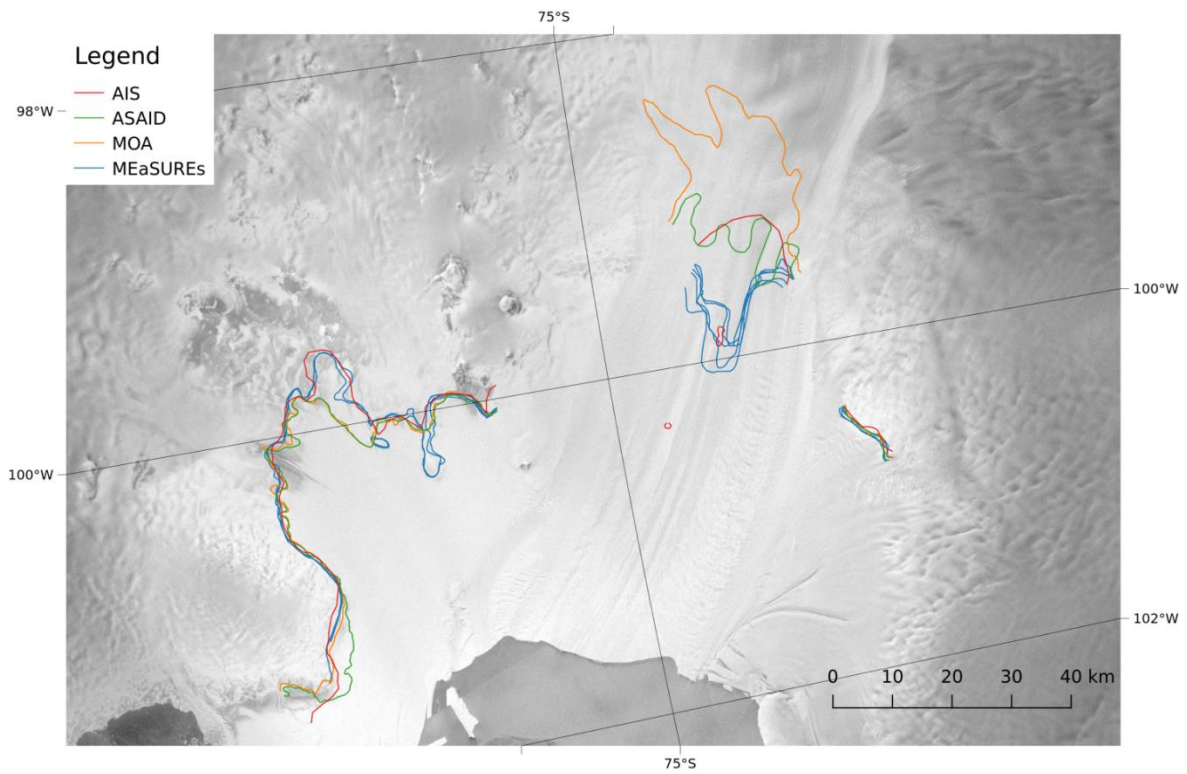
Figure 4-7: The PIG area with all validation GLLs and the AIS GLL derived from ERS-1/2 data.
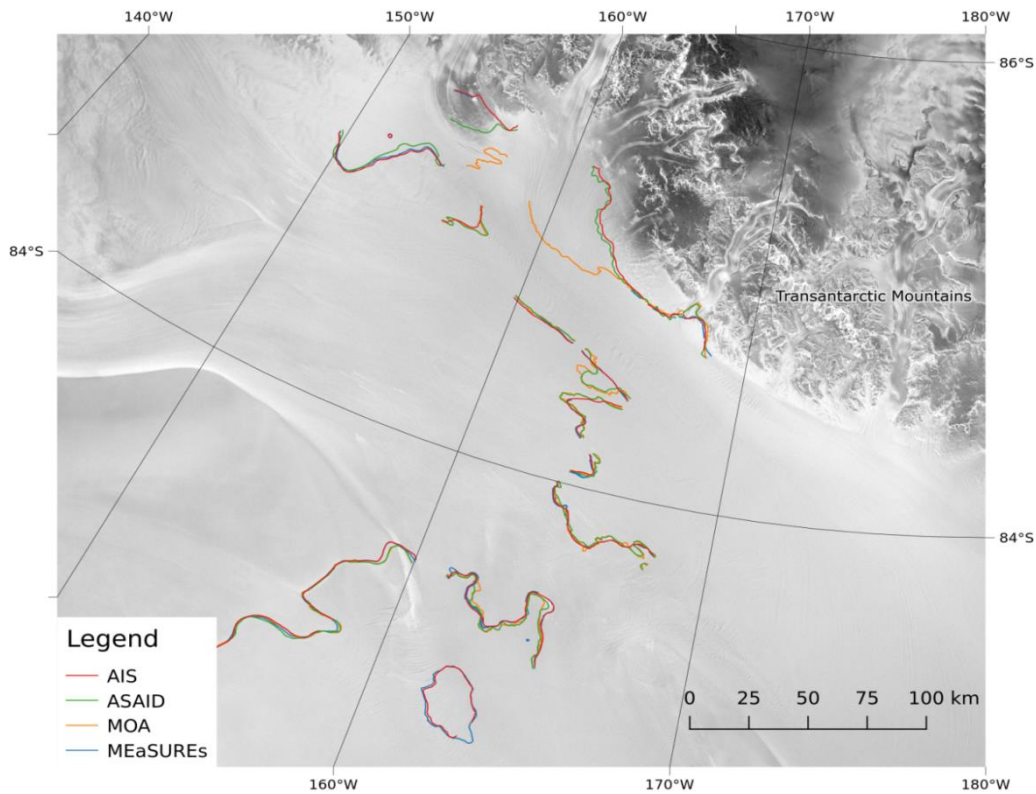
Figure 4-8: The TAM area (Southern Ross Ice Shelf and Transantarctic Mountains) with all validation GLLs and the AIS_cci GLL derived from TerraSAR-X data.

To quantify the differences among the various GLLs a polygon comparison procedure has been adapted to project's needs and has been implemented for the purpose of validation. All selected validation lines and our product are represented as two-dimensional polylines. Polylines are collection of points with a defined connection.

A problem which occurs if two polylines are compared is that there is no defined mapping between the points belonging to the reference line and those belonging to the target line, respectively. Moreover, the sampling of both polylines may differ significantly. This implies that a distance between points cannot automatically be calculated for each point without defining a line-to-line (or point-to-point) assignment. One solution which provides a mapping between two lines is the assumption that for each point on the target line, the closest point found on the reference line is the corresponding point. It is important to note, that even if the same mapping technique is used the result of the assignment may vary depending on which lines are selected as target and reference, respectively.

A good way to visualise minimal distances around a line is to create a region around it, we call this object a buffer. One example of using a buffer around a polyline is shown in

Figure 4-9. The buffers around the AIS_cci GLL, defined as reference line, are increased until the target line (ASAID GLL) is completely contained within the buffer (e.g. at 5000 m distance). The overlap with the target line can be calculated for each buffer distances. These buffers can then be used to calculate the overlap (expressed in percentage) with other lines at a specific distance.
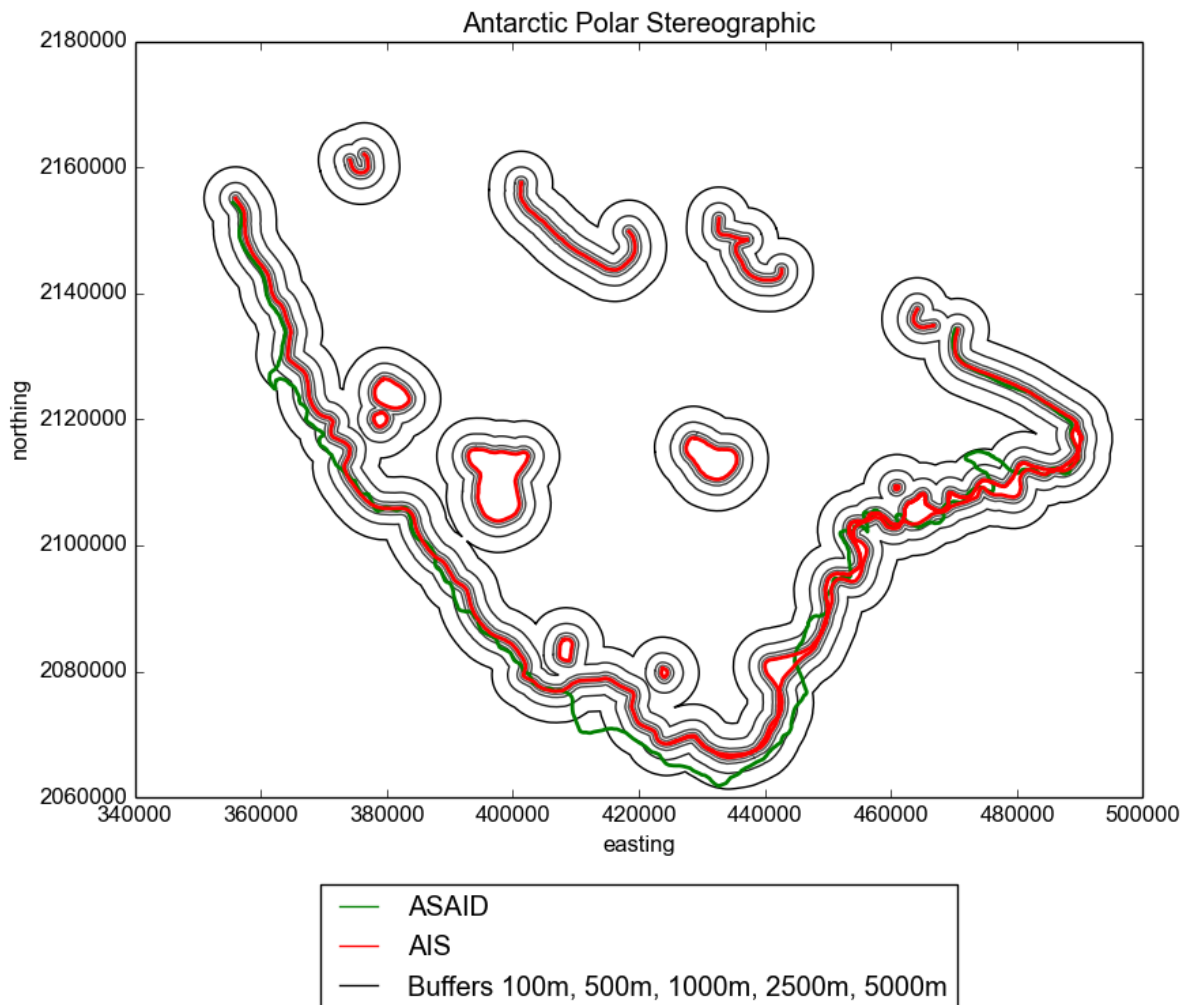
Figure 4-9: Buffers (black lines) corresponding to different distances around the AIS_cci GLL (reference line, in red). The target line is the ASAID GLL (in green). At the largest distance of 5000m the green line is almost completely contained within the buffer**.**

very small steps in order to get more precise results. Because of this we decided for a more generic approach – a proximity image – which is simply another implementation. The reference polyline is represented in a binary image and the shortest distance for each pixel in the image to the reference line is determined and stored as value at this

point. The spatial sampling of that image is 5 m x 5 m which therefore is the smallest detectable difference. Such a proximity image is shown in

Figure **4-10**.

All datasets which shall be validated are now equally resampled and superimposed onto this image. Depending on the shape of the polyline these datasets will cross different "distance values" of the proximity image. All the values which will be encountered if one traverses along the GLL of the validation dataset result in a histogram (left side plots on Figure 4-11 to Figure 4-15). The more values obtain shorter distances, the better the final fit will be. Besides the histogram characteristics, the mean values of the distances also quantify the equality between two polylines and are given in Table 4-1.

In order to show how well the target lines are approximated by the AIS_cci we also determine, how much of the other curve is covered by the reference curve within a predefined buffer size. This step is repeated for different continuously growing buffer sizes. A plot of the overlap (in percentage) against the buffer size is generated for each of the target lines in each of the validation sites. This is called a Cumulative Ratio Curve (CRC) and is similar to a Cumulative Density Function of a distribution (Heo 2009), (Jeong 2013). The CRCs are shown on the right-side plots of Figure 4-11 to Figure 4-15.
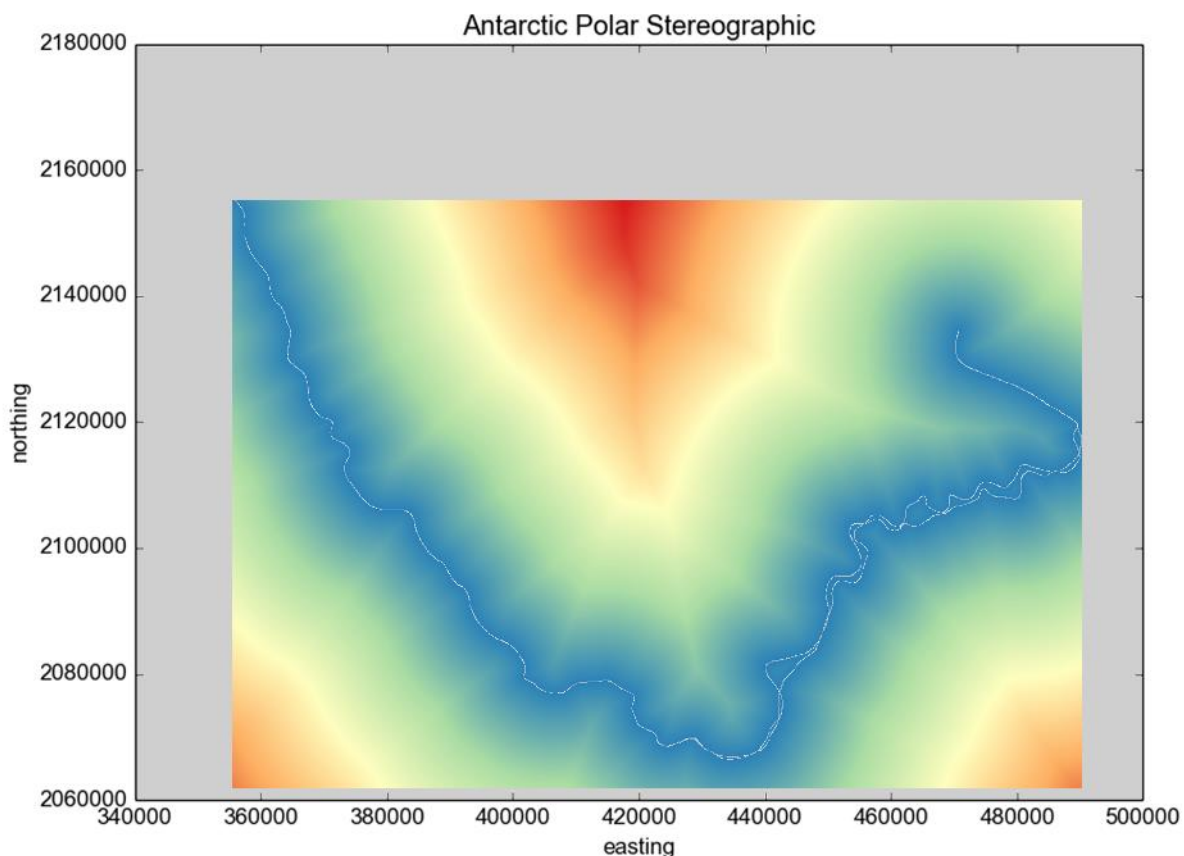

Figure 4-10: Proximity image for AIS_cci GLL at Schirmacher derived from ERS. The color scale from blue-green-yellow-red depicts increasing distances to the polyline. The white line is the reference AIS_cci GLL.

4.3 Validation outcome

We performed the validation procedure on each of the four areas by comparing the AIS_cci GLLs with the independent validation dataset. Each comparison yields an average minimal distance between the lines which represents the mean value of "difference" between the participating lines (Table 4-1). For each comparison the histograms and CRC curves described in Section 4.2 were generated (Figure 4-11 to Figure 4-15). In addition, we compared a segment of the grounding line which was generated from the same SAR dataset within two different projects, MEaSUREs and AIS_cci (Section 4.3.5).

Table 4-1: Mean of the distances between the AIS_cci GLL and the respective validation candidates.

	d_{ASAID} [m]	d_{MOA} [m]	$d_{MEaSUREs}$ [m]
Schirmacher ERS	1372	1481	599
Schirmacher S1	782	1056	688
Brunt/Caird	666	953	446
PIG	1871	5625	3649
TAM	2039	4016	573
Average (all areas)	1328	2626	1191
Average (excl. PIG)	1215	1877	576

In the PIG area the mean distances AIS_cci vs. MEaSUREs have to be interpreted with care because the MEaSUREs dataset contains a time series of GLLs which vary significantly in locations (up to 12 km). In this case the overlap ratio is < 1 even for big buffer sizes and reaches 1 at distances much larger than the 5000 m.

4.3.1 Schirmacher area

Schirmacher ERS
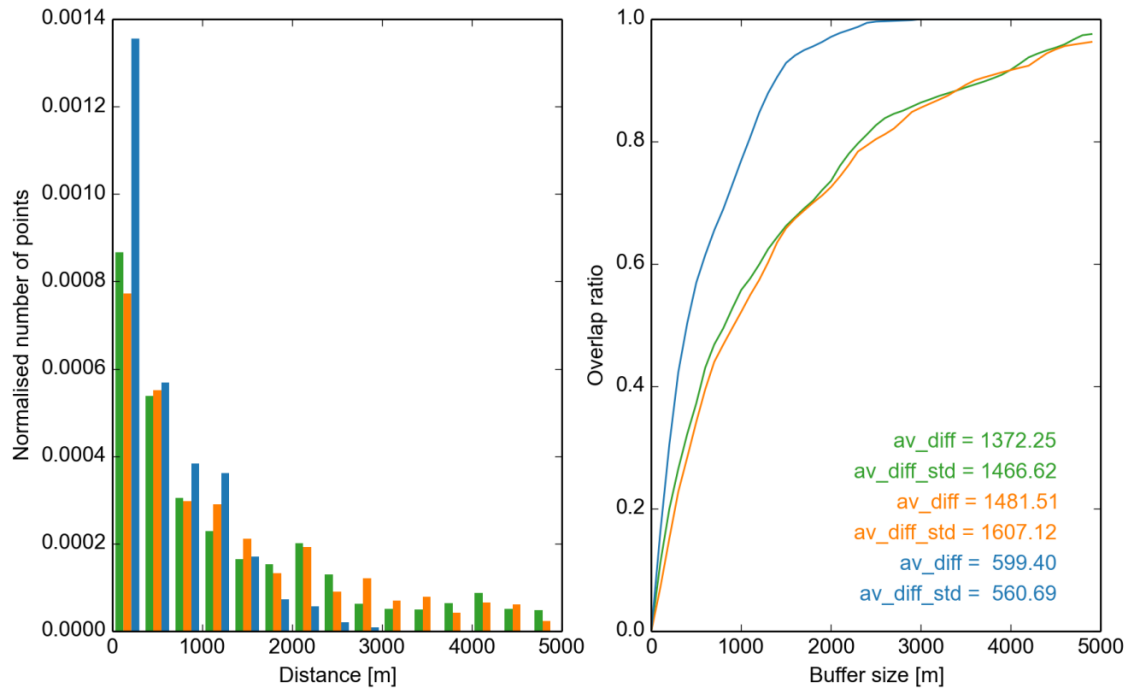
Figure 4-11: Comparison of the AIS_cci GLL line in the Schirmacher area derived from ERS data with the validation GLL: AIS_cci vs. ASAID (green), MOA (orange) and MEaSUREs (blue). Left: histogram of the distances between the GLL lines. The number of points is normalised with respect to the area below the curve. Right: the Cumulative Ratio Curve.

Schirmacher Sentinel-1

Figure 4-12: Same as Figure 4-11 but in the Schirmacher area. The AIS_cci GLL was derived from Sentinel-1 data.

4.3.2 Brunt/Caird

Figure 4-13: Same as Figure 4-11 but in the Brunt/Caird area. The AIS_cci GLL was determined from ERS-1/2 data.

4.3.3 PIG

Figure 4-14: Same as Figure 4-11 but in the PIG area.

4.3.4 TAM

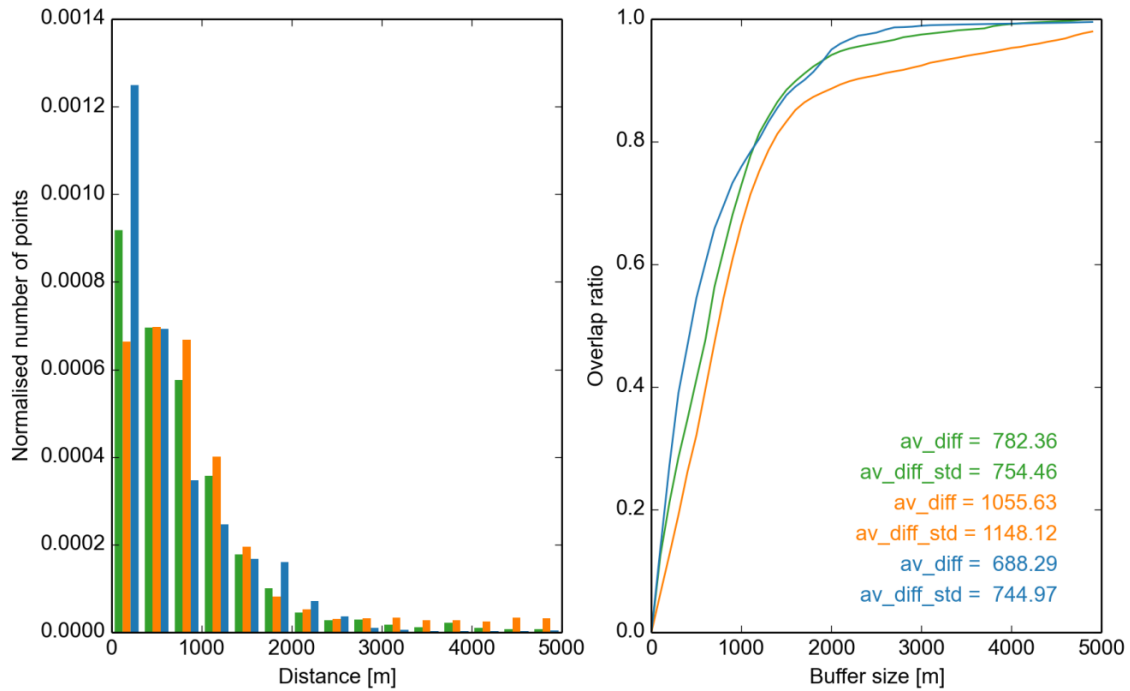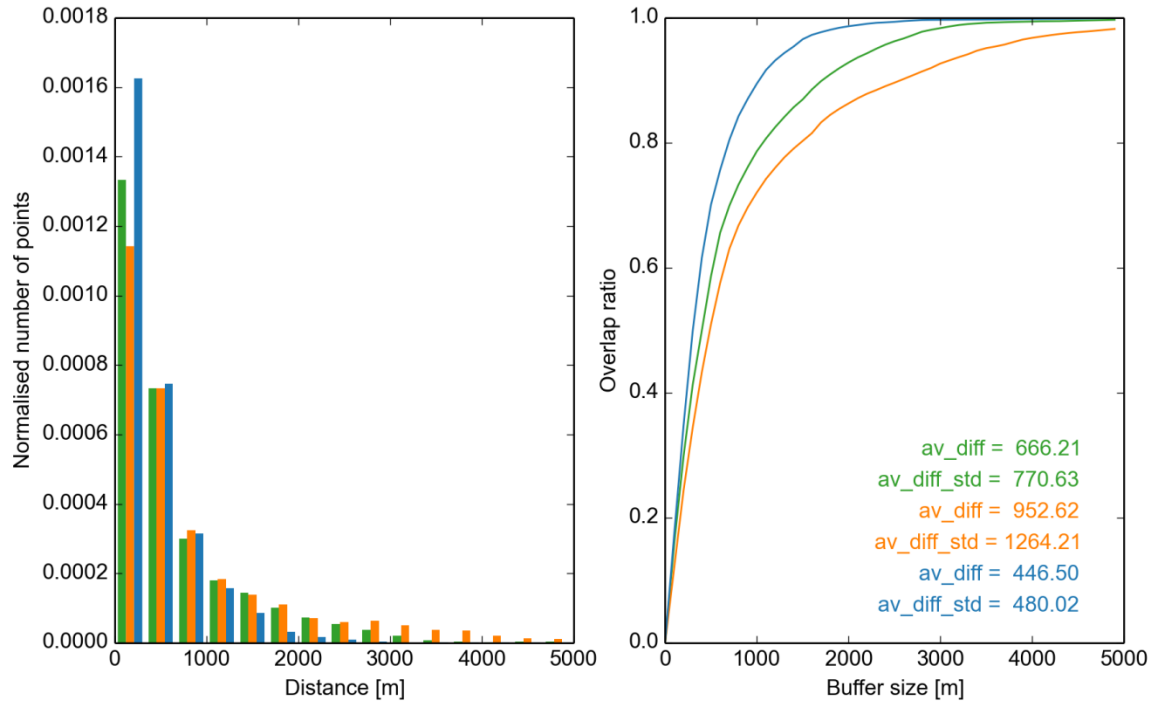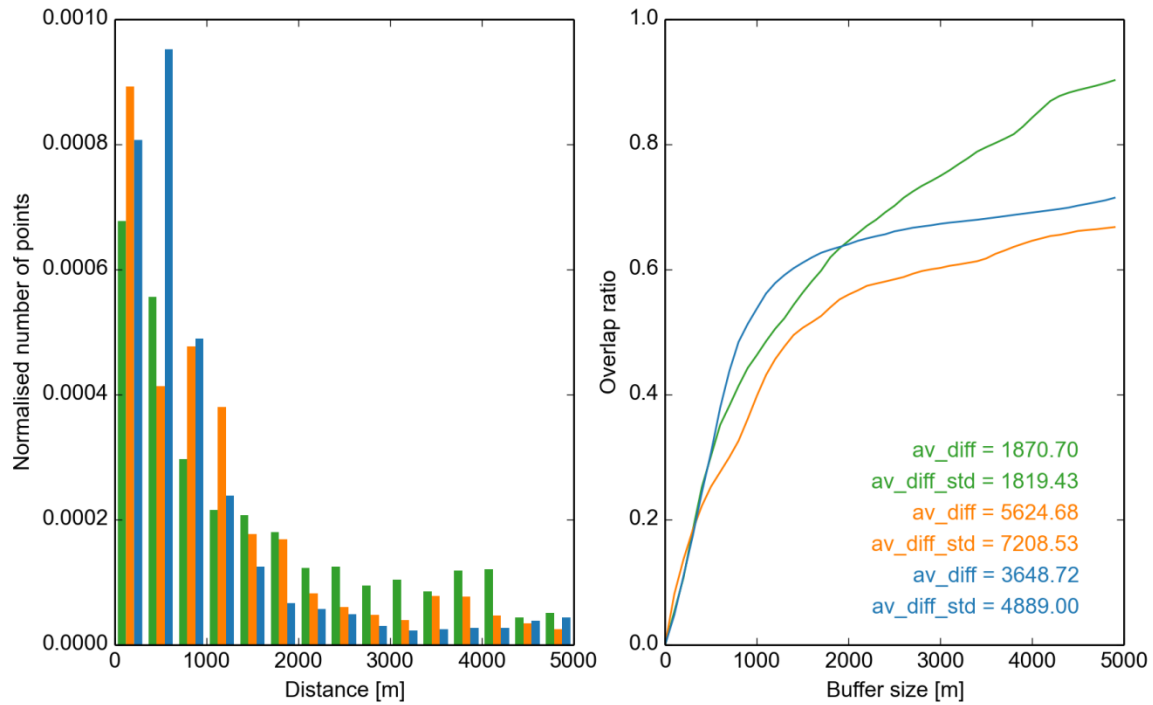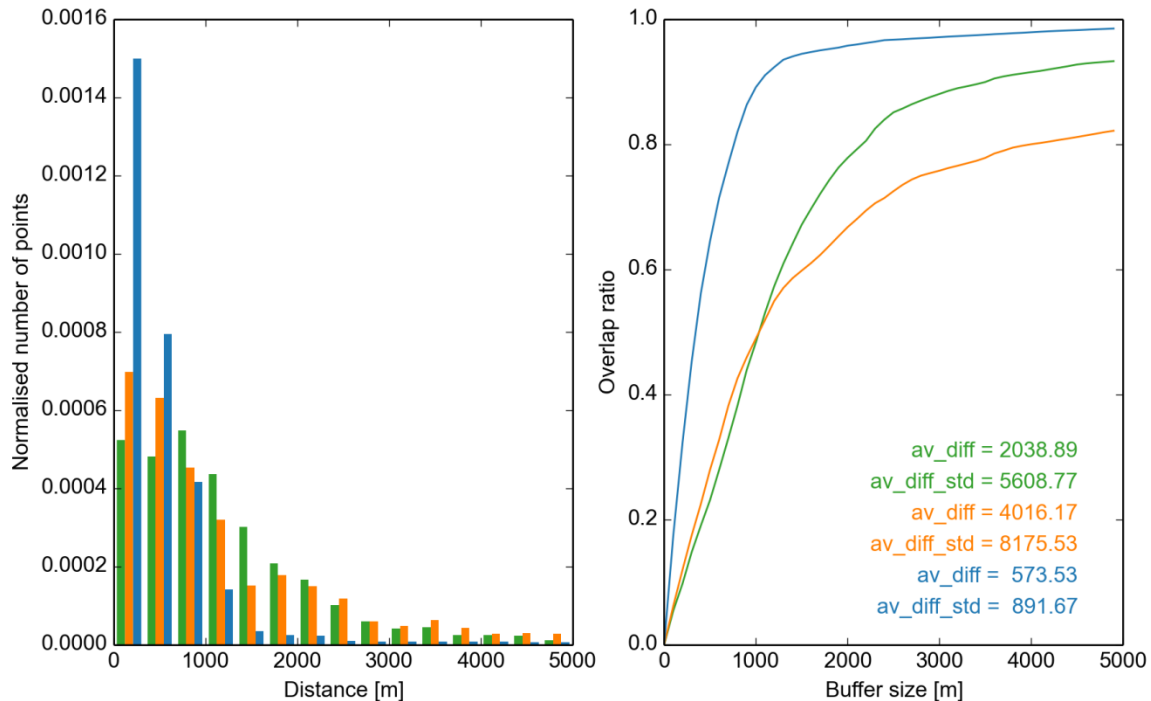**Figure 4-15:** Same as Figure 4-11 but in the TAM area. The AIS_cci GLL was obtained from TerraSAR-X data.

4.3.5 Identical SAR datasets: MEaSUREs vs. AIS_cci

For a validation that takes temporal variation of the GLL into account, we compare two AIS_cci GLLs against grounding lines generated within the MEaSUREs project (Rignot et al., 2011b), (Scheuchl et al., 2016). In contrast to the comparisons shown above, this validation only concerns grounding line segments that have been produced from identical SAR acquisitions. In particular, we carry out two comparisons:

1. both AIS_cci and MEaSUREs GLLs were created from Sentinel-1A satellite data acquired on the dates 2014-11-23, 2014-12-05 and 2014-12-17 (Figure 4-16a)

2. both AIS_cci and MEaSUREs GLLs were created from ERS-1 satellite data acquired on the dates 1994-03-04, 1994-03-07 and 1994-03-11 during the 2nd Ice Phase (Figure 4-16b)

By using the identical SAR acquisitions, temporal variations between AIS_cci GLLs and MEaSUREs GLLs due to tide level variations or grounding line retreat are excluded. The differences of the GLLs reflect the spatial accuracy of the grounding line delineation using the same methodology. Therefore, we expect smaller mean differences between these GLLs than in the comparison of the validation GLL products presented in sections 4.3.1

to 4.3.4. From the visual inspection in Figure 4-16 it is obvious that both AIS_cci and MEaSUREs GLLs are overlapped well on Dotson/ Crosson Ice Shelves and Jutulstraumen Glacier. Just in some areas on Dotson/ Crosson Ice Shelves neither AIS_cci GLL nor MEaSURE GLL could be derived.

(a)

(b)
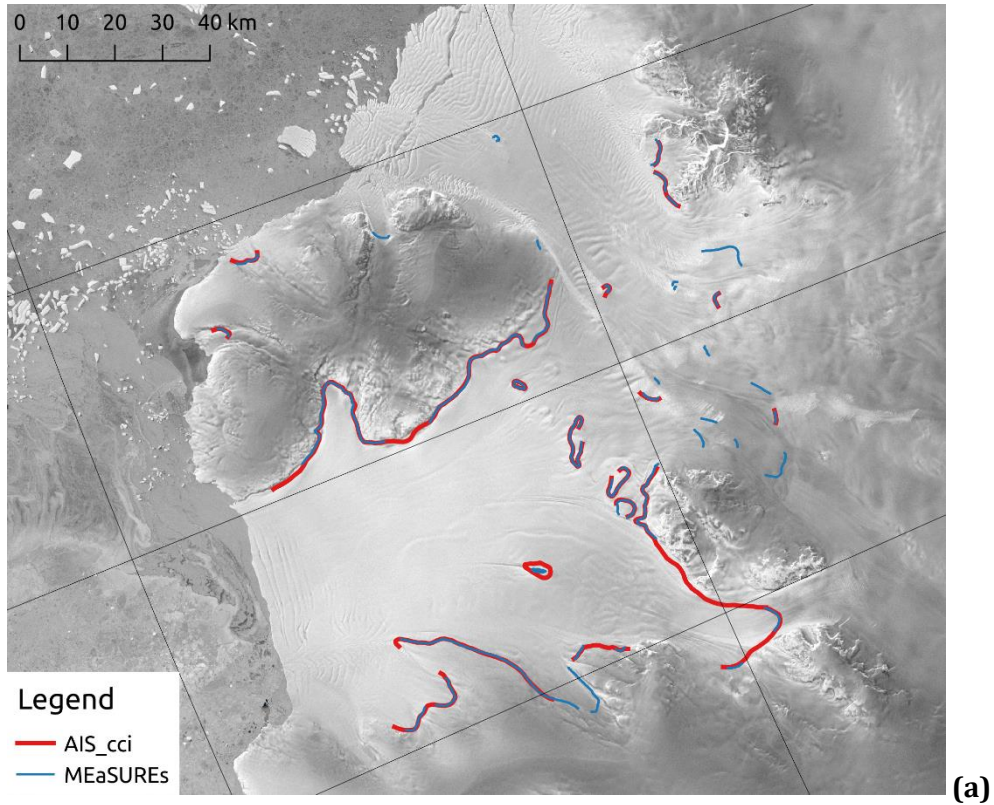
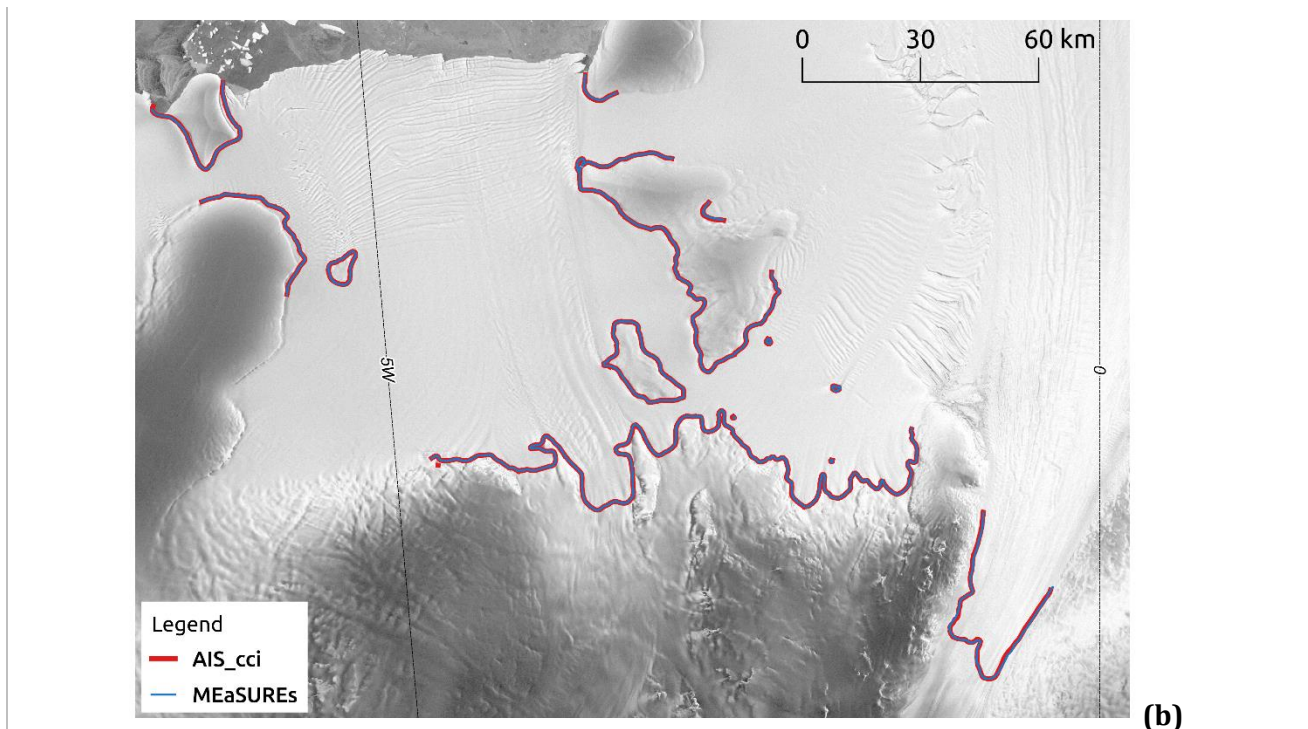**Figure 4-16:** AIS_cci (red) and MEaSUREs (blue)GLL segments in (a) the Dotson/Crosson Ice Shelves area generated from the Sentinel 1A data triplet acquired on 2014-11-23/ 2014-12-05/ 2014-12-17 and (b) Jutulstraumen Glacier area generated from the ERS-1 triplet acquired on 1994-03-04/ 1994-03-07/ 1994-03-11.

We use the same methodology that was applied in the previous comparisons as a metric to report spatial differences of the GLLs. This time however, the comparison is done bidirectional, meaning that distances from each point defining the AIS_cci GLLs to the MEaSUREs GLLs are calculated and vice versa. The full comparison results are shown in Figure 4-17 to Figure 4-19. In Figure 4-17 all GLL segments, which are generated from identical Sentinel-1A triplet, are compared to each other even if they don't have a matching counterpart in the other dataset, while in Figure 4-18 and Figure 4-19 only GLL segments derived from Sentinel-1A and ERS-1 showing in both datasets are compared.

The two GLL products are following each other very well. Within a 500m buffer distance around the AIS_cci GLL 79% of the MEaSUREs GLL can be explained (red line in Figure 4-17 right). The fact that this ratio doesn't increase significantly with a growing buffer size means that about 20% of the MEaSUREs GLL has no matching counterpart in the AIS_cci dataset.

Similar is observed for the MEaSUREs GLL that has about 76% overlap with the AIS_cci dataset within the first 500m (blue line in Figure 4-17 right). The overlap increase at higher buffer distances is due to the fact that missing parts of the MEaSUREs dataset are often a continuation of the lines detected in AIS_cci GLL, whereas the parts that are missing from the AIS_cci dataset mostly stem from individual MEaSUREs GLL segments that are often far from other GLLs (see Figure 4-16a).
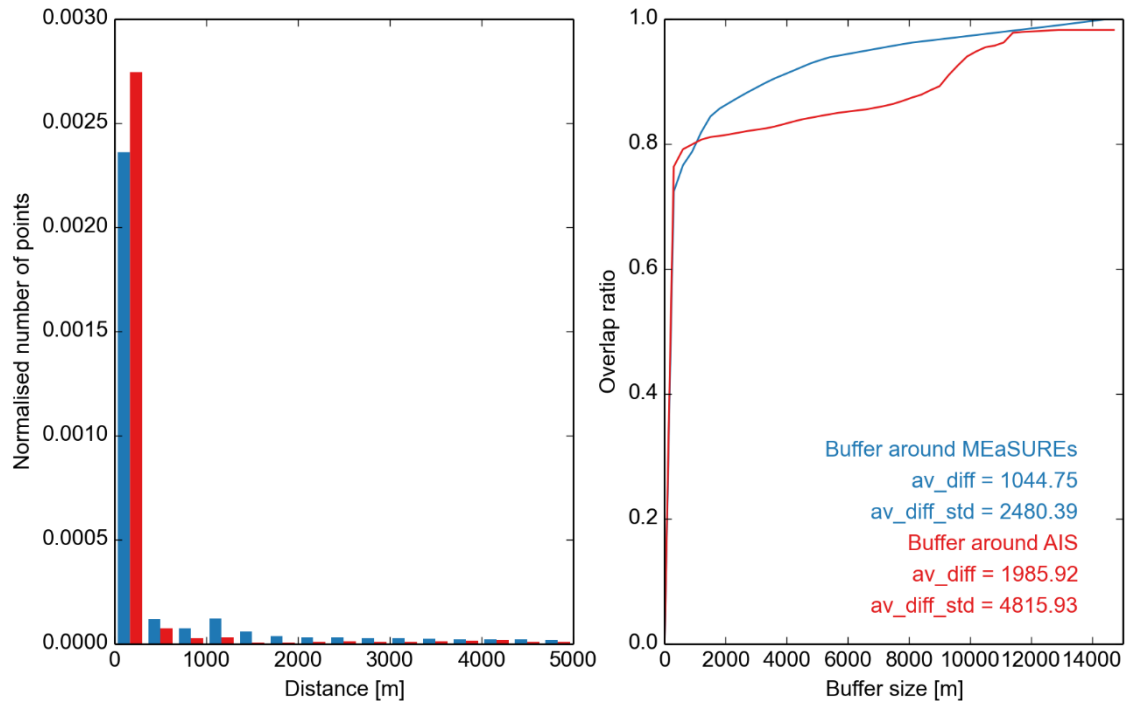
Figure 4-17: The bidirectional comparison results for GLL from identical Sentinel-1A acquisitions. All line segments are compared to each other. Left: histogram of the distances between the GLL lines. Right: Red line results when the distance from each point of MEaSUREs GLL to the closest point of AIS_cci GLL is calculated. Blue line results when the distance from each point of AIS_cci GLL to the MEaSUREs GLL is calculated.

To better assess the similarity of both GLLs, we only include GLL segments that have a mean distance of less than 5000m to its closest counterpart and therefore disregard line segments that don't have a matching representation in the other dataset. In Figure 4-18 we show the results and report mean distances of 129 and 173m for the two directions of comparison, respectively. As expected, there is now an almost complete overlap of the GLLs within small buffer distances. The remaining non-overlap is caused by line segments which have a small mean distance and are therefore included in the comparison, but that contain a number of points that have no matching counterpart. These are mostly line continuations where one candidate ends earlier than the other.

In Figure 4-19 the comparison is done between the GLLs which are derived from the ERS-1 triplet on Jutulstraumen Glacier. The bidirectional comparison shows that the mean distance is between 55 and 59m. Both GLLs are completely overlapped within 500m buffer distances.
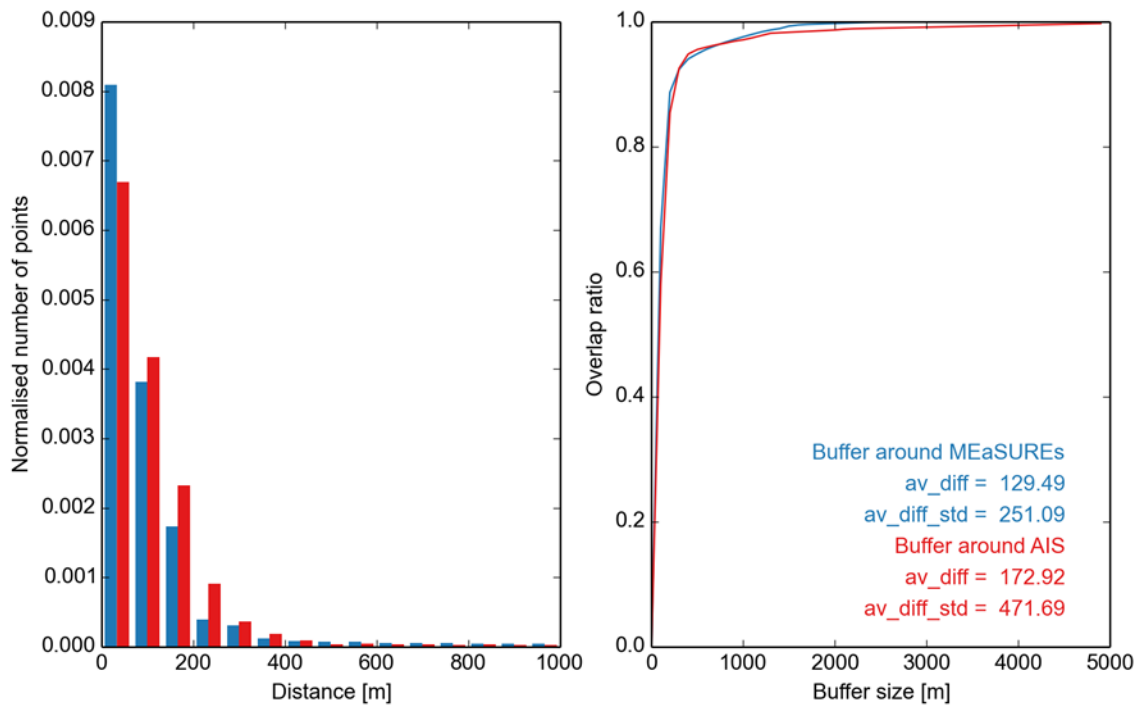
Figure 4-18: Same as Figure 4-17 but only GLL segments generated from Sentinel-1A data having counterparts in the two datasets are considered.
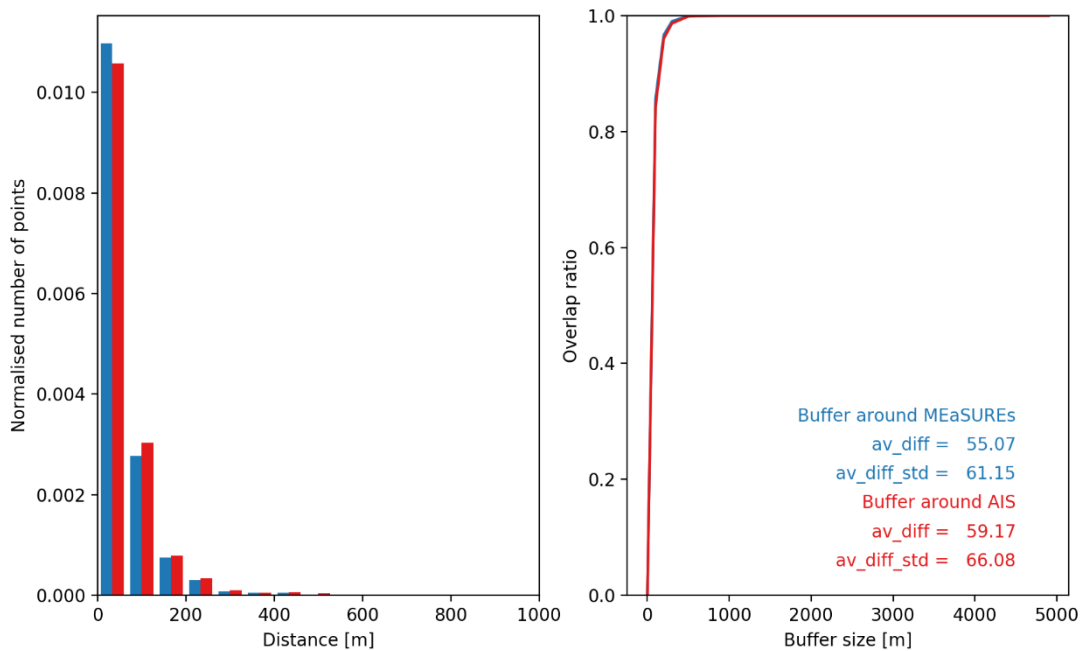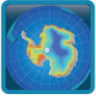

Figure 4-19: Same as Figure 4-18 (GLL has counterparts in both datasets) but for GLL segments generated from ERS-1.

4.3.6 Interpretation and explanation of validation outcome

Table 4-1 shows the mean distances of AIS_cci vs. ASAID, MOA and MEaSUREs for each investigated area as well as the overall average distances for each dataset (when all regions are included). In addition, the average distances were also determined without PIG area since we think the time series contained in PIG MEaSUREs dataset biases the result and makes it worse than it actually is. One has to bear in mind that ocean tides were not considered or corrected in any of the used datasets and shifts in GLL within one tidal cycle can reach up to 10 km if either tides are strong or the subglacial topography is gentle.

The comparison of all validation datasets reveals that MEaSUREs and AIS_cci match best, in average with 576 m which is an extremely good agreement. It was expectable though that results which utilize the same methodology would provide similar results. ASAID is the next best fit with an average distance of 1.2 km, while MOA's average distance is 1.8 km. The histograms itself enable a more detailed understanding of which accuracy bands are represented in which dataset to which extent.

Regarding the comparison of the AIS_cci GLLs processed from the same Sentinel-1A and ERS-1 datasets the small values of the mean distances validate our products with respect to the MEaSUREs grounding line. Remaining differences can be caused by various error sources as e.g. differences in InSAR processing or fringe delineation. The differences are however in a range that is to be expected and can be accepted for an indirect measurement of the GLL. A more thorough validation of the actual spatial accuracy of the GLL can only be achieved by comparing in situ measurements of the GLL.

4.4 Recommendations for product improvement

There are currently no recommendations for product improvement.

4.5 Acknowledgements of data contributors for GLL validation
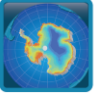
The following datasets were used for the present validation:

Haran, T., J. Bohlander, T. Scambos, T. Painter, and M. Fahnestock. 2005, updated 2013. MODIS Mosaic of Antarctica 2003-2004 (MOA2004) Image Map, Version 1. [Indicate subset used]. Boulder, Colorado USA. NSIDC: National Snow and Ice Data Center. doi: http://dx.doi.org/10.7265/N5ZK5DM5. [Accessed February 2016].

Bindschadler, R., H. Choi, and ASAID Collaborators. 2011. High-resolution Image-derived Grounding and Hydrostatic Lines for the Antarctic Ice Sheet. Boulder, Colorado, USA: National Snow and Ice Data Center. http://dx.doi.org/10.7265/N56T0JK2.

Rignot, E., J. Mouginot, and B. Scheuchl. 2011b. Antarctic Grounding Line Mapping from Differential Satellite Radar Interferometry, *Geophyical Research Letters*. 38. L10504. https://doi.org/10.1029/2011GL047109

Rignot, E., J. Mouginot, and B. Scheuchl. 2016. *MEaSUREs Antarctic Grounding Line from Differential Satellite Radar Interferometry, Version 2*. [Indicate subset used]. Boulder,

Colorado USA. NASA National Snow and Ice Data Center Distributed Active Archive Center. doi: http://dx.doi.org/10.5067/IKBWW4RYHF1Q. [Accessed March 2017].

Scheuchl, B., J. Mouginot, E. Rignot, M. Morlighem, and A. Khazendar (2016), Grounding line retreat of Pope, Smith, and Kohler Glaciers, West Antarctica, measured with Sentinel-1a radar interferometry data, Geophys. Res. Lett., 43, 8572–8579, doi:10.1002/2016GL069287.

Mohajerani Y, Jeong S, Scheuchl B, Velicogna I, Rignot E, Milillo P. Automatic delineation of glacier grounding lines in differential interferometric synthetic-aperture radar data using deep learning. Sci Rep. 2021;11(1):4992. Published 2021 Mar 2. doi:10.1038/s41598-021-84309-3

5 Gravimetric Mass Balance (GMB)

This chapter gives a complete report on the activities carried out to assess the quality of the GMB products. All assessments make use of the first CCI+ Climate Research Data Package (CRDP), published via the AIS_cci GMB data portal (data1.geo.tu-dresden.de/ais_gmb). The data package relies on the GRACE/GRACE-FO monthly solution series CSR RL06 provided by the Center for Space Research (University of Texas at Austin) (Bettadpur 2018, Save 2019) and covers the period 2002-04 – 2020-07. The utilised GRACE series CSR RL06 includes spherical harmonic coefficients up to degree l_{max}=96, although we only made use of the coefficients until degree 90. Figure 5-1 shows the mass balance pattern (i.e. the linear trend) derived from the entire time series.

5.1 Independent validation data

5.1.1 Requirements

An ideal validation data set would consist of an independent observation of the quantity to be validated, carried out by an alternative sensor, which is more precise and provides an identical spatial coverage at higher spatial resolution. In case of the GMB data set the validation data are required to provide observations of the change in ice mass with a temporal resolution of one month and a spatial resolution better than 50 km, while covering the entire AIS.
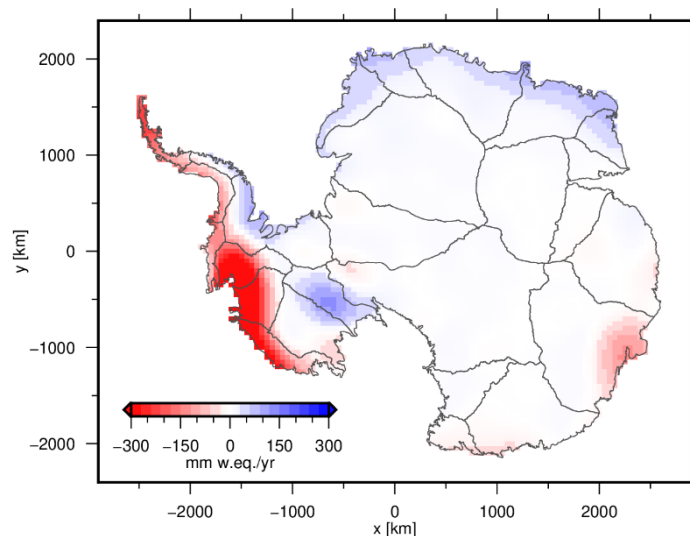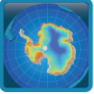
Figure 5-1: Spatial pattern of the linear trend in ice mass during the period 2002-04 – 2020-07.

Unfortunately, no sensor except of GRACE is able to directly observe changes in mass with a comparable or even better spatial and temporal coverage. Hence, observations of alternative quantities related to mass changes have to be used after applying an appropriate conversion. For example, changes in the ice sheet's surface elevation can be converted into mass changes using an assumption of the density. The validation could also be based on the predictions of geophysical models. All these alternatives have the

drawback of being dependent on additional assumptions and input data with their individual uncertainties.

5.1.2 Sources

Three major types of data sets are suitable for the GMB product validation. The following provides a brief description of the three data sets. An inter-comparison of results based on these types of data as well as on GRACE/GRACE-FO satellite gravimetry is given by Shepherd et al., (2018).

SEC

Surface elevation changes (SEC) of the AIS have been observed by different types of satellite altimetry missions, carrying laser (ICESat) or radar instruments (e.g. CryoSat-2). Satellite altimetry allows the precise mapping of SEC patterns, whereas radar altimetry provides the longest record with a monthly temporal sampling. Shepherd et al., (2019) compiled a SEC time series spanning the period from 1992 to 2017 from cross-calibrated observations of the radar satellites ERS-1, ERS-2, ENVISAT and CryoSat-2.
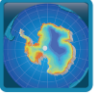
Averaged over a certain drainage basin, volume changes need to be converted into mass changes in order to make them comparable to GMB products. Different approaches are used for this purpose. One approach makes use of a prescribed density model to discriminate between regions where fluctuations in elevation occur with the density of snow or ice (McMillan et al., 2014, Shepherd et al., 2019). Other studies make use of a firn compaction model (Ligtenberg et al., 2011) forced by a regional climate model (van Wessem et al., 2014) to correct SEC observations for fluctuations in the firn layer thickness.

SMB

Surface mass balance (SMB), defined as the difference between the mass gained by precipitation and the mass lost by sublimation and run-off, is one component of the ice sheets total mass balance (van den Broeke et al., 2011). Fluctuations in SMB can be predicted by regional climate models at high spatial (10-30 km) and temporal resolution (monthly) (Lenaerts et al., 2012), like the widely used model RACMO (van Wessem et al., 2014). For regions where the mass balance is dominated by changes in SMB, modelled cumulated SMB anomalies can be used for the inter-comparison with GMB time series.

IOM

The Input-output method (IOM) relies on the combination of mass input at the surface and mass loss through ice discharge into the ocean (van den Broeke et al., 2011). Information on the mass input is inferred from modelled fluctuations in SMB, while the mass loss component is derived from ice velocity and ice thickness information. For example, yearly ice velocity estimates can be derived from interferometric synthetic-aperture radar data. Ice thickness may be derived by radar echo sounding or by using satellite altimetry in combination with the hydrostatic equilibrium of the floating ice shelves (Rignot et al., 2011c). After interpolating the slowly change discharge estimates,

monthly mass balance estimates can be derived on the scale of individual drainage basins or for the entire AIS.

5.1.3 Assessment

Each of the three data sets introduced in the previous section comes with its individual strengths and weaknesses. For a comprehensive overview on the individual uncertainties cf. Shepherd et al., (2018) and references therein.

SEC observations may be biased by variations in the radar signal penetration into the firn layer. However, by far the largest uncertainties in SEC-based mass change time series arise from the conversion between volume and mass. Although the SEC patterns are provided at high spatial resolution, the polar gap prevents a complete coverage of the AIS.

Predicted fluctuations in SMB largely depend on the atmospheric forcing used as model input. Different global atmospheric reanalyses data sets used for SMB modelling yield significant differences in the model predictions. Consequently, these uncertainties are propagated to derived products, like firn densification models used in SEC processing.

IOM results are very sensitive to uncertainties in both components, i.e. modelled fluctuations in SMB and observed ice velocity and thickness (van den Broeke et al., 2011).

5.1.4 Selection
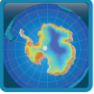
Considering the limited number of possible data sets suitable for the GMB product validation and the limitations of each of these data sets, a comprehensive validation needs to be based on the entire range of available sources. Unfortunately, only a few data sets are freely available. The following data sets could be used in the GMB quality assessment:

1. A SEC-based mass change time series for different drainage basins and aggregations derived from radar altimetry observations were provided by UL. The conversion from volume to mass was achieved using the density model described in Shepherd et al., (2019). This time series covers the period 1992 – 2018 and allows the inter-comparison with the corresponding time series from the GMB basin product (cf. PUG).

2. Monthly time series of basin-averaged cumulative SMB anomalies were derived from SMB predictions according to the regional climate model RACMO2.3 (van Wessem et al., 2014) with a spatial resolution of 27 km x 27 km. The entire time series covers the period between 1979 and 2020.

3. IOM time series for selected drainage basins and aggregations are provided by Velicogna et al., (2020).

5.2 Validation procedure

Since only three external data sets are available, the GMB quality assessment also comprises the inter-comparison of results based on different GRACE releases as well as

results derived from synthetic data sets. In this way the performance of the selected algorithm, the quality of the utilised GRACE/GRACE-FO release and the overall quality of the final GMB products are proven. The following test and inter-comparisons were conducted.

A. **GRACE releases**: The noise level of the monthly solutions from different GRACE releases is investigated. At this stage residuals w.r.t. a linear and seasonal modelled are analysed. The analysis is done in the spherical harmonic domain using the median degree amplitudes ($\sigma_l = sqrt[\sum_{m=0}^{l}(C_{lm}^2 + S_{lm}^2)]$). In the spatial domain the median of all monthly residual maps is utilized to illustrate the noise level. For this purpose, the monthly maps are smoothed using a Gaussian filter with a half-width of 400 km. Preliminary investigations revealed that the GRACE/GRACE-FO releases exhibiting the lowest noise level are provided by CSR (RL06) and by TU Graz (ITSG-Grace2018). Hence, the inter-comparisons shown in the following section are limited to 157 monthly solutions between 2002 and 2020 common to these releases.

In addition, mass change time series for selected drainage basins and aggregations are compared. The design of the sensitivity kernels used for the regional integration depends on empirical GRACE error variance-covariances inferred from the respective GRACE series in use (Groh & Horwath, 2021). Hence, the sensitivity kernels differ between the releases.

B. **Synthetic data**: The utilized algorithm (Groh & Horwath, 2021) is applied to a range of synthetic data sets with a priori known mass changes. By comparing the derived mass change estimates with the true mass changes, conclusion on the performance of the algorithm and induced signal leakage can be drawn. The synthetic data sets used are identical to those utilized for the Round Robin experiment (Groh et al., 2019).

C. **SEC**: Mass change time series for different drainage basins and aggregations are compared w.r.t. their overall agreement and their individual mass balance estimates. The mass balance (i.e., the linear trend) is derived by fitting a linear, periodic (1 year, 1/2 year) and quadratic model to the period common to both time series.

D. **IOM**: Mass change time series for aggregations of drainage basins are compared w.r.t. their overall agreement and their individual mass balance estimates. The mass balance (i.e., the linear trend) is derived by fitting a linear, periodic (1 year, 1/2 year) and quadratic model to the period common to both time series.

E. **SMB**: Since the basin-averaged accumulated SMB anomaly time series solely represent the surface component of the total mass change, a direct comparison to the GMB basin product is not possible. Ice discharge shows only negligible seasonal variations and is clearly dominated by long-term signals. To ensure comparability, long-term signals (linear and quadratic) are removed from both the SMB and the GMB time series. The residual seasonal and inter-annual variations

are mainly due to fluctuations in SMB. Correlations between both residual time series are used as indicators for the level of agreement.

5.3 Validation outcome

A. **GRACE releases**: Figure 5-2 shows the median degree amplitudes of the residuals derived from CSR RL06 and ITSG-Grace2018 series. For spherical harmonic degrees larger than 15 the degree amplitudes for ITSG-Grace2018 exhibit less power, indicating a lower noise level. At higher degrees, which are dominated by errors, this difference becomes even larger. The same is true for the degree amplitudes calculated for spherical harmonic order m=0…29, only. Coefficients of these orders are of particular importance for studies in polar region. The differences in noise level between the two releases are clearly reduced compared to their precursors (i.e., CSR RL05 and ITSG-Grace2016).
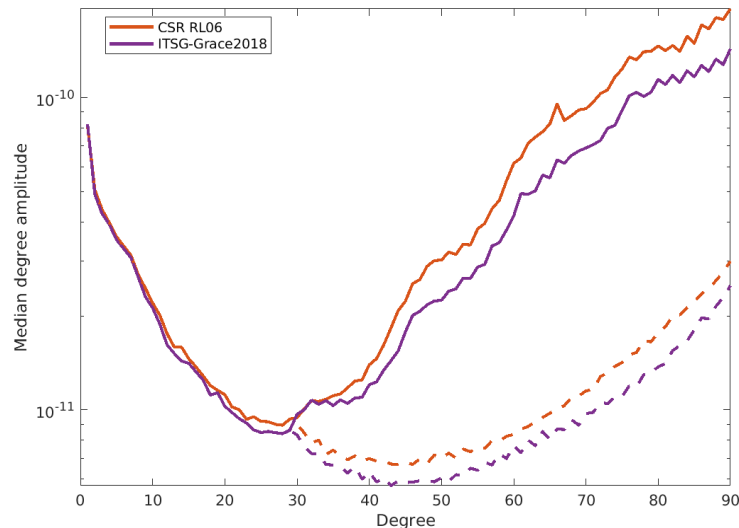
Figure 5-2: Median degree amplitudes of residual Stokes coefficients (solid lines). Dashed lines: Median degree amplitudes for order m=0…29.

The spatial patterns of the median residuals are shown in Figure 5-3. Conclusions on the noise level can be derived by inspecting those regions apart from the prominent mass signals, e.g., the global oceans and the AIS interior. For the interior of the AIS the median residuals for ITSG-Grace2018 are slightly smaller than for CSR RL06. Moreover, the region of low noise is larger and extended further towards the coast. Over the oceans, the differences between both releases are also visible. Somewhat smaller striping artefacts are evident in the ITSG-Grace2018 results. Results based on a weaker smoothing, e.g., a Gaussian filter with 200 km half-width, reveal even larger differences between the releases, which is in agreement with the median degree amplitudes shown in Figure 5-2.

	Antarctica_Ice_Sheet_cci+ Product Validation and Intercomparison Report (PVIR)	Reference : ST-UL-ESA-AISCCI+-PVIR-001 Version : 1.0 page Date : 01 October 2021 55/63

antarctic ice sheet cci
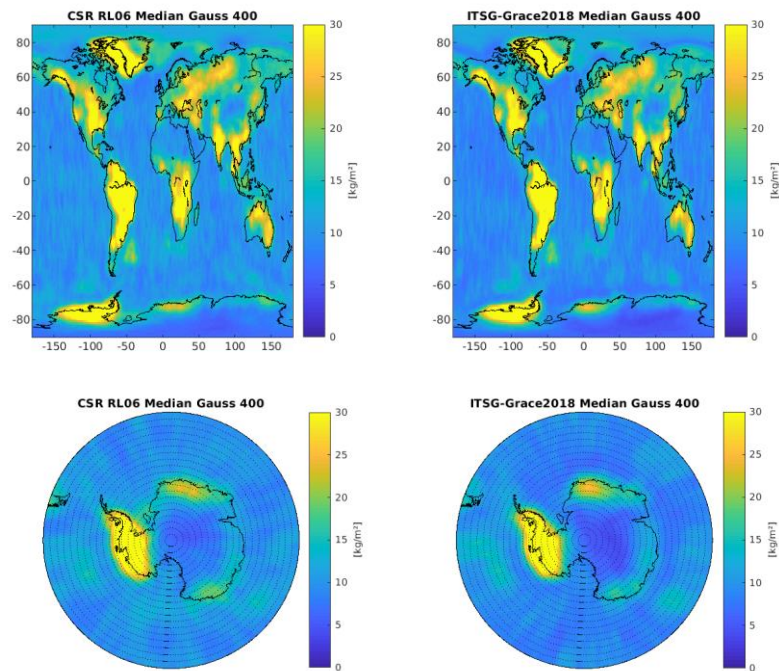
Figure 5-3: Global (top) and regional (bottom) maps of median residuals from CSR RL06 (left) and ITSG-Grace2018 (right) monthly GRACE/GRACE-FO series.

The different noise levels of the releases are also visible in the mass change time series for different aggregations of drainage basins shown in Figure 5-4. However, these differences are small and long-term, inter-annual and seasonal signals are comparably revealed by both solution series.

In summary, the assessment of the noise level suggests utilising the GRACE/GRACE-FO series ITSG-Grace2018. Nevertheless, we decided to make use of the CSR RL06 solutions for the GMB product generation. This is solely because the GRACE solutions of the ITSG-Grace2018 series following 2016-08 (until 2017-06, the period during which the accelerometer on board of one of the GRACE satellites had to be switched off) exhibit a clearly increased noise level for some coefficients, especially the low-degree zonal harmonics (e.g., C_{30}). This is of particular importance for studies on regions around the poles, e.g., the AIS, and leads to exceptionally large outliers in the mass change time series (not shown in Figure 5-6). Since the differences between the two-solution series are small for the remaining periods, and since we want to avoid shortening the time series, we decided to choose CSR RL06. This decision will be re-evaluated once new data release are available.
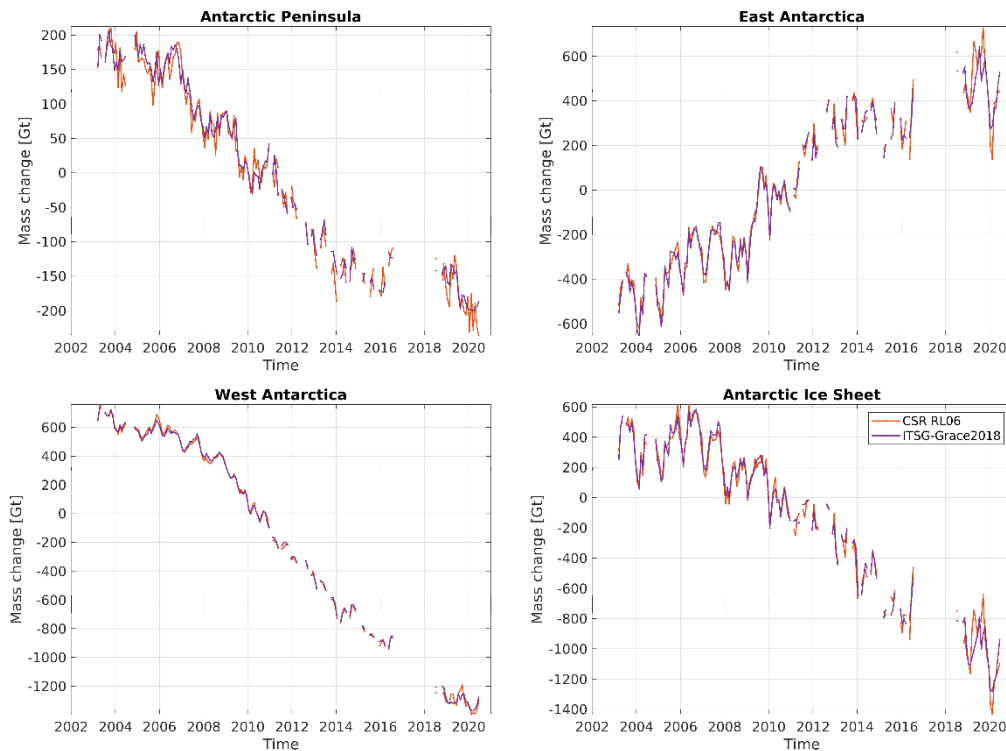
Figure 5-4: Mass change time series for the Antarctic Peninsula, East Antarctica, West Antarctica and the entire AIS derived from CSR RL06 and ITSG-Grace2018 GRACE/GRACE-FO solutions.

B. **Synthetic data**: The overall performance of the applied algorithm was demonstrated in the Round Robin experiment (Groh et al., 2019). Meanwhile, further modifications were adopted to the algorithm in order to find the optimal compromise between the minimisation of both GRACE/GRACE-FO error effects and signal leakage (Groh & Horwath, 2021). The updated synthetic results are given in Figure 5-5. For example, the leakage error induced by the spatial pattern of the mean annual mass change of the AIS (data set number 7 – "AIS MB") is below 1 Gt, corresponding to about 1% of the true mass change.
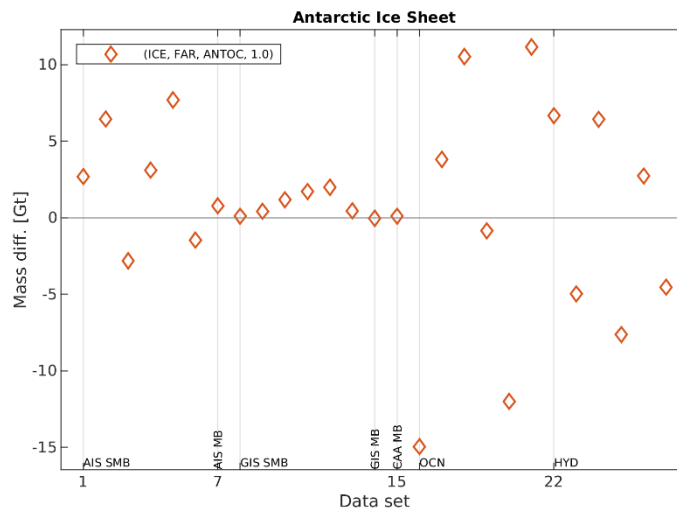
Figure 5-5: Differences between the mass changes derived from synthetic data sets and the corresponding synthetic 'true' mass change for the entire AIS (AIS32). The bottom row indicates the type of synthetic data set (Groh & Horwath, 2021).

C. **SEC**: The comparison of the SEC- and GRACE-derived mass change time series for basin aggregations in Dronning Maud Land and the Amundsen Sea Sector is given in Figure 5-6. The mass loss in the Amundsen Sea Sector (West Antarctica) is revealed by both techniques. Larger differences are visible for Dronning Maud Land (East Antarctica), where the mass gain caused by two larger accumulation events in 2009 and 2011, is more pronounced in the GMB time series. The linear trend estimates over the period 2002-04 – 2016-08 given in Table 5-1 confirms the general better agreement for drainage basins exhibiting a negative mass balance (e.g. AIS21-AIS23) compared to basins with positive mass balance (e.g. AIS04-AIS08). However, considering the uncertainties inherent to each technique (Groh & Horwath, 2021), none of the time series can be preferred over the other, making it difficult to perform a rigorous product validation.

D. **IOM**: For the period 2002-04 – 2016-08, the mass balance estimates for the Amundsen Sea Sector derived from GMB (-105.0±14.1 Gt/yr) and IOM (-121.2±8 Gt/yr) agree with the corresponding uncertainties. Larger discrepancies are revealed for Dronning Maud Land, where the IOM rate (28.5±13 Gt/yr) is in better agreement with the SEC (21.6±01.4 Gt/yr) than with GMB (48.2±04.7 Gt/yr).

We used both the SEC and the IOM time series to check for a seamless continuation of the GRACE time series by GRACE-FO and for the existence of a potential gap. For this purpose, we assume that all three products just differ by a bias in the linear trend. Hence, we reduced the individual linear trends over the GRACE period 2002-04–2016-08 from each data set and compared the residuals with respect to this linear trend over the GRACE-FO period. Figure 5-6(faint lines) does not indicate a potential offset between the GRACE and GRACE-FO results in the GMB product. However, due to the uncertainties of the individual data sets

and the varying discrepancies in the trend over different time periods, the SEC and IOM data do not provide a suitable reference for a rigorous assessment of the GMB product.
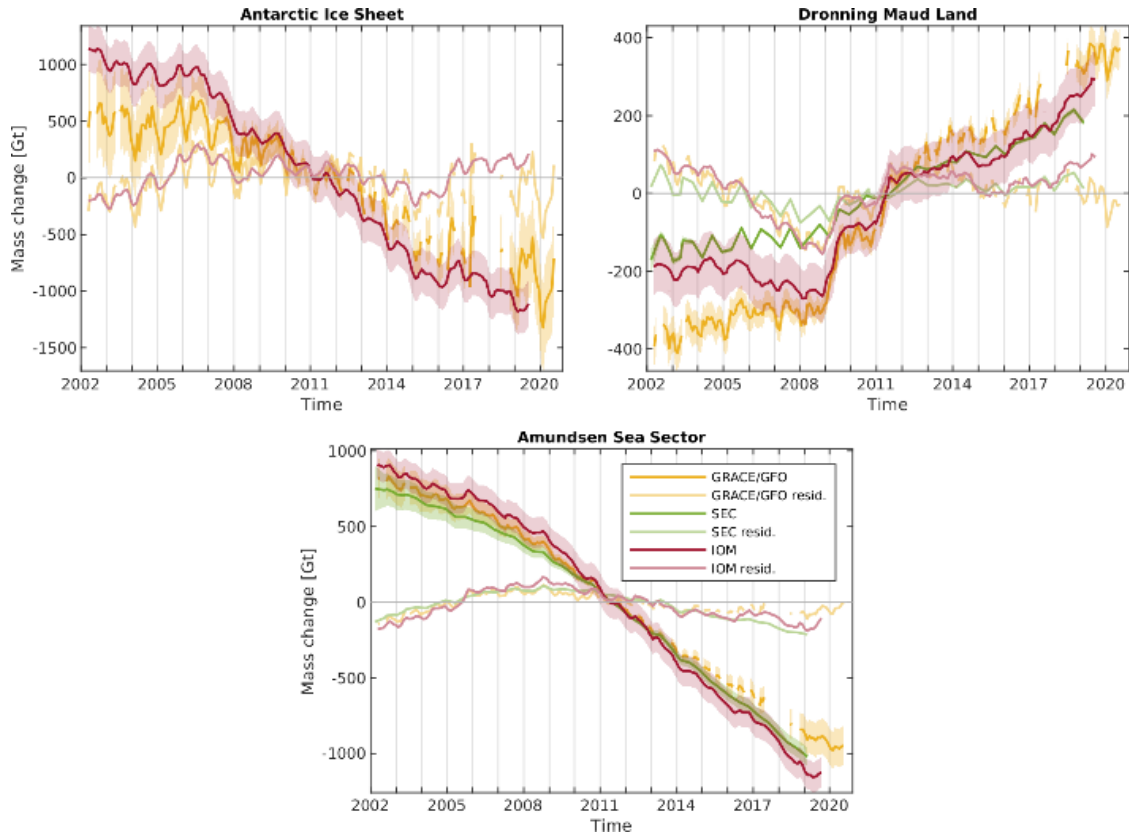
Figure 5-6: Mass change time series the Antarctic Ice Sheet, Dronning Maud Land (Basins 21-22) and the Amundsen Sea Sector (Basins 5-8) derived from GRACE/GRACE-FO (CSR RL06), SEC and IOM data. Faint lines indicate the corresponding residuals with respect to the linear trend over the period from 2002-04 through 2016-08.

Table 5-1: Linear trends for the period 2002-04-2016-08, derived from the GMB and SEC mass change time series. Basin IDs in bold indicate agreement between the GMB and SEC rates with the corresponding uncertainties.

Basin ID	Linear trend GMB [Gt/yr]	Linear trend SEC [Gt/yr]	Basin ID	Linear trend GMB [Gt/yr]	Linear trend SEC [Gt/yr]
AIS01	5.1±05.7	5.1±02.1	AIS14	-7.3±03.5	-4.9±01.0
AIS02	2.8±04.5	1.8±06.2	AIS15	-3.7±00.7	-2.6±00.8
AIS03	16.7±14.1	6.8±00.6	AIS16	1.2±01.0	0.7±00.3
AIS04	11.0±02.4	3.8±00.6	AIS17	6.7±06.9	5.1±00.8
AIS05	7.1±00.9	3.6±00.6	AIS18	15.0±03.9	11.4±01.5

AIS06	17.5±02.4	6.9±00.8	AIS19	0.9±03.0	0.1±00.8
AIS07	16.9±03.8	7.7±00.9	AIS20	-36.5±05.8	-25.6±04.0
AIS08	6.7±01.1	3.4±00.5	AIS21	-54.9±09.0	-59.6±07.2
AIS09	1.3±01.4	1.1±00.5	AIS22	-50.1±10.9	-42.2±06.2
AIS10	3.8±06.2	-0.2±00.8	AIS23	-9.7±05.0	-6.2±02.1
AIS11	-0.4±02.2	-0.7±00.4	AIS30	72.9±39.1	14.3±05.5
AIS12	4.9±04.1	-2.3±01.3	AIS31	-130.2±15.0	-116.8±12.1
AIS13	-12.4±02.9	-15.2±02.0			

E. **SMB**: Figure 5-7 compares residual mass change time series from RACMO2.3p2 and GRACE/GRACE-FO for selected drainage basins and aggregations. The differences in the high-frequent signal components, mainly caused by noise in the GMB series, hampers a direct comparison, in particular for basins with small fluctuations in SMB. Low-pass filtered time series are more suitable to study the agreement between both data sets. Time series for the larger aggregations (Antarctic Peninsula, East Antarctica, West Antarctica) exhibit comparable seasonal and inter-annual variations. Pronounced signals, like caused by the 2009
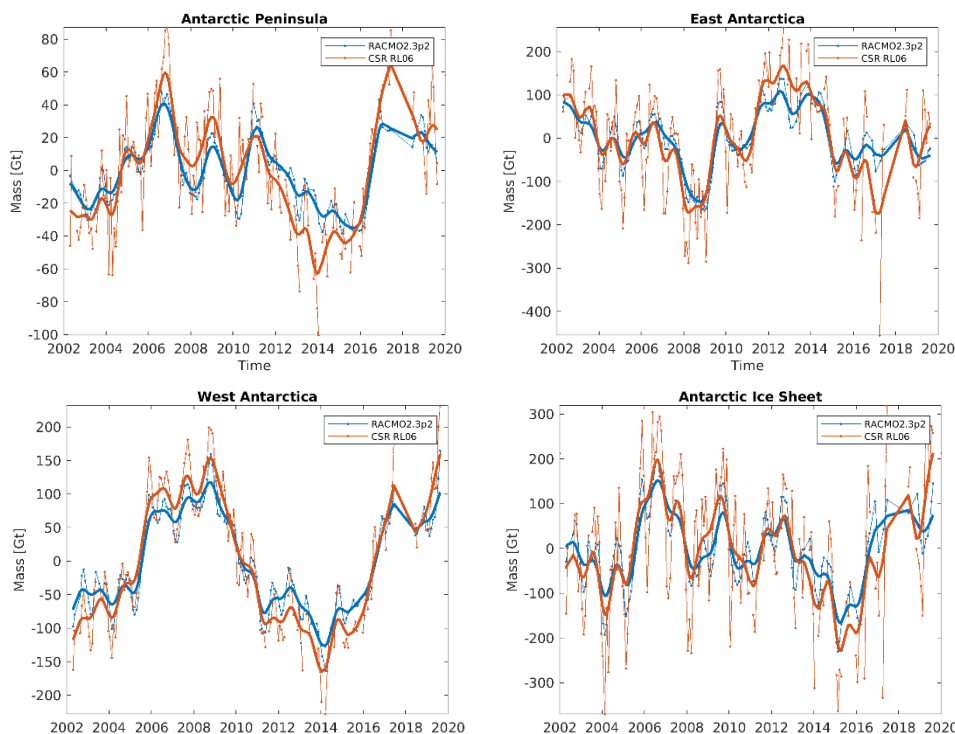

Figure 5-7: Residual mass change time series from RACMO2.3p2 and GRACE/GRACE-FO (thin lines) for selected aggregations. Linear and quadratic signal components are removed. Bold lines: Low-pass filtered time series.

and 2011 accumulation events in Dronning Maud Land, are equally revealed by both series (cf. East Antarctica).
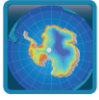
The correlation coefficients listed in Table 5-2 indicate the general good agreement between the results from GRACE/GRACE-FO and RACMO2.3p2. By nature, the majority of basins reveal an increased level of agreement for the low-pass filtered results. Only for a few smaller basins, exhibiting low variations in SMB, no correlation is found between the two time series (cf. AIS27).

Table 5-2: Correlation coefficients between the time series of residual mass changes from RACMO2.3p2 and GRACE/GRACE-FO.

Basin ID	Correlation original time series	Correlation low-pass filtered time series	Basin ID	Correlation original time series	Correlation low-pass filtered time series
AIS01	0.770	0.894	AIS16	0.392	0.682
AIS02	0.481	0.619	AIS17	0.622	0.855
AIS03	0.709	0.925	AIS18	0.378	0.588
AIS04	0.751	0.943	AIS19	0.827	0.951
AIS05	0.671	0.924	AIS20	0.959	0.989
AIS06	0.913	0.990	AIS21	0.856	0.916
AIS07	0.816	0.977	AIS22	0.889	0.943
AIS08	0.447	0.811	AIS23	0.770	0.817
AIS09	0.425	0.714	AIS24	0.897	0.957
AIS10	0.416	0.589	AIS27	0.020	0.037
AIS11	0.438	0.760	AIS28	0.555	0.773
AIS12	0.714	0.824	AIS29	0.780	0.908
AIS13	0.748	0.866	AIS30	0.795	0.922
AIS14	0.839	0.959	AIS31	0.966	0.989
AIS15	0.450	0.821	AIS32	0.782	0.919

5.4 Recommendations for product improvement

Future algorithm improvements will focus on the incorporation of more realistic GRACE error information, e.g., by using actual GRACE/GRACE-FO variance/co-variances matrices instead of empirical estimates. Moreover, to further improve the GMB product validation, it will be necessary to extend the existing archive of external data sets, e.g., by means of SEC-based time series for the Antarctic Peninsula.

5.5 Acknowledgements of data contributors for GMB validation

We acknowledge the support by UL and the Institute for Marine and Atmospheric Research Utrecht (IMAU) who provided SEC mass change time series and fluctuations in SMB predicted by RACMO2.3p2, respectively.

6 References

British Antarctic Survey (2005). Antarctic factsheet geographical statistics. British Antarctic Survey, Natural Environment Research Council. https://www.bas.ac.uk/wp-content/uploads/2015/05/factsheet_geostats_print.pdf (last access April 2016)

Bettadpur, S. (2018). GRACE UTCSR Level-2 Processing Standards Document for Level-2 Product Release 0006, v5.0; Technical Report; Center for Space Research, The University of Texas at Austin: Austin, TX, USA.

Bindschadler, R., H. Choi, A. Wichlacz, R. Bingham, J. Bohlander, K. Brunt, H. Corr, R. Drews, H. Fricker, M. Hall, R. Hindmarsh, J. Kohler, L. Padman, W. Rack, G. Rotschky, S. Urbini, P. Vornberger, and N. Young. 2011. Getting around Antarctica: New High-Resolution Mappings of the Grounded and Freely-Floating Boundaries of the Antarctic Ice Sheet Created for the International Polar Year. The Cryosphere, 5, 569-588. doi:10.5194/tc-5-569-2011.

Flament, T. and F. Remy (2012). Antarctica volume change from 10 years of Envisat altimetry. Conference paper, International Geoscience and Remote Sensing Symposium (IGARSS), 2012 IEEE International. doi: 10.1109/IGARSS.2012.6351149.

Groh, A., Horwath, M., Horvath, A., Meister, R., Sørensen, L. S., Barletta, V. R., Forsberg, R., Wouters, B., Ditmar, P., Ran, J., Klees, R., Su, X., Shang, K., Guo, J., Shum, C. K., Schrama, E., & Shepherd, A. (2019). Evaluating GRACE Mass Change Time Series for the Antarctic and Greenland Ice Sheet—Methods and Results. Geosciences, 9(10), 415. doi:10.3390/geosciences9100415.

Groh, A., & Horwath, M. (2021). Antarctic Ice Mass Change Products from GRACE/GRACE-FO Using Tailored Sensitivity Kernels. Remote Sens., 13(9), 1736. doi:10.3390/rs13091736.

van den Broeke, M., Bamber, J., Lenaerts, J., & Rignot, E. (2011). Ice Sheets and Sea Level: Thinking Outside the Box. Surv. Geophys., 32(4), 495–505.

Burton-Johnson, A., Black, M., Fretwell, P. T., and Kaluza-Gilbert, J.: An automated methodology for differentiating rock from snow, clouds and sea in Antarctica from Landsat 8 imagery: a new rock outcrop map and area estimation for the entire Antarctic continent, The Cryosphere, 10, 1665-1677, https://doi.org/10.5194/tc-10-1665-2016, 2016.

Heo, J., Kim, J.H. and Kim, J.W., 2009. A new methodology for measuring coastline recession using buffering and non-linear least squares estimation. *International Journal of Geographical Information Science*, *23*(9), pp.1165-1177.

Jeong, S., Jung, J., Kim, S., Hong, S., Sohn, H.G. and Heo, J., 2014. Buffering-based approach to fluctuation analysis of glacier calving fronts using LANDSAT-7 ETM+, with a case study of Jakobshavn Isbræ. *Computers & Geosciences*, *64*, pp.115-125.

Lenaerts, J. T. M., van den Broeke, M. R., van de Berg, W. J., van Meijgaard, E., & Kuipers Munneke, P. (2012). A new, high-resolution surface mass balance map of Antarctica (1979-2010) based on regional atmospheric climate modeling. Geophys. Res. Lett., 39(4), L04501.

Ligtenberg, S. R. M., Helsen, M. M., & van den Broeke, M. R. (2011). An improved semi-empirical model for the densification of Antarctic firn. The Cryosphere, 5(4), 809–819.

Mayer-Gürr, T., Behzadpour, S., Ellmer, M., Kvas, A., Klinger, B., & Zehentner, N. (2016). ITSG-Grace2016 – Monthly and Daily Gravity Field Solutions from GRACE. GFZ Data Services, doi:10.5880/icgem.2016.007

McMillan, M., Shepherd, A., Sundal, A., Briggs, K., Muir, A., Ridout, A., Hogg, A., & Wingham, D. (2014). Increased ice losses from Antarctica detected by CryoSat-2. Geophys. Res. Lett., 41(11), 3899–3905.

Mouginot, J., E. Rignot, B. Scheuchl, and R. Millan. 2017a. Comprehensive Annual Ice Sheet Velocity Mapping Using Landsat-8, Sentinel-1, and RADARSAT-2 Data, Remote Sensing. 9. Art. #364. https://doi.org/10.3390/rs9040364

Mouginot, J., B. Scheuchl, and E. Rignot. 2017, updated 2017b. MEaSUREs Annual Antarctic Ice Velocity Maps 2005-2017, Version 1. [Indicate subset used]. Boulder, Colorado USA. NASA National Snow and Ice Data Center Distributed Active Archive Center. doi:10.5067/9T4EPQXTJYW9.

Rignot, E., J. Mouginot and B. Scheuchl (2011a). "Ice Flow of the AIS." Science 333 (6048): 1427-1430

Rignot, E., J. Mouginot, and B. Scheuchl. (2011b). Antarctic Grounding Line Mapping from Differential Satellite Radar Interferometry, Geophysical Research Letters. 38. L10504. doi:10.1029/2011GL047109.

Rignot, E., Velicogna, I., van den Broeke, M. R., Monaghan, A., & Lenaerts, J. (2011c). Acceleration of the contribution of the Greenland and Antarctic ice sheets to sea level rise. Geophys. Res. Lett., 38(5), L05503.

Rignot, E., J. Mouginot, and B. Scheuchl. 2017. MEaSUREs InSAR-Based Antarctica Ice Velocity Map, Version 2. Boulder, Colorado USA. NASA National Snow and Ice Data Center Distributed Active Archive Center. doi: http://dx.doi.org/10.5067/D7GK8F5J8M8R. [3 May 2017].

Save, H. (2019). GRACE-FO CSR Level-2 Processing Standards Document for Level-2 Product Release 06, v1.1. Technical Report; Center for Space Research, The University of Texas at Austin: Austin, TX, USA.

Scambos, T., T. Haran, M. Fahnestock, T. Painter, and J. Bohlander. 2007. MODIS-based Mosaic of Antarctica (MOA) Data Sets: Continent-wide Surface Morphology and Snow Grain Size. Remote Sensing of Environment 111(2): 242-257. http://dx.doi.org/10.1016/j.rse.2006.12.020.

Shepherd, A., Ivins, E., Rignot, E., Smith, B., van den Broeke, M., Velicogna, I., Whitehouse, P., Briggs, K., Joughin, I., Krinner, G., Nowicki, S., Payne, T., Scambos, T., Schlegel, N., A, G., Agosta, C., Ahlstrøm, A., Babonis, G., Barletta, V., Blazquez, A., Bonin, J., Csatho, B., Cullather, R., Felikson, D., Fettweis, X., Forsberg, R., Gallee, H., Gardner, A., Gilbert, L., Groh, A., Gunter, B., Hanna, E., Harig, C., Helm, V., Horvath, A., Horwath, M., Khan, S., Kjeldsen, K. K., Konrad, H., Langen, P., Lecavalier, B., Loomis, B., Luthcke, S., McMillan, M., Melini, D., Mernild, S., Mohajerani, Y., Moore, P., Mouginot, J., Moyano, G., Muir, A., Nagler, T., Nield, G., Nilsson, J., Noel, B., Otosaka, I., Pattle, M. E., Peltier, W. R., Pie, N., Rietbroek, R., Rott, H., Sandberg-Sørensen, L., Sasgen, I., Save, H., Scheuchl, B., Schrama, E., Schröder, L., Seo, K. - W., Simonsen, S., Slater, T., Spada, G., Sutterley, T., Talpe, M., Tarasov, L., van de Berg, W. J., van der Wal, W., van Wessem, J. M., Vishwakarma, B. D., Wiese, D., & Wouters, B. (2018). Mass balance of the Antarctic Ice Sheet from 1992 to 2017. Nature, 558(7709), 219–222. doi:10.1038/s41586-018-0179-y.

Shepherd, A., Gilbert, L., Muir, A. S., Konrad, H., McMillan, M., Slater, T., Briggs, K. H., Sundal, A. V., Hogg, A. E., & Engdahl, M. (2019). Trends in Antarctic Ice Sheet Elevation and Mass. Geophys. Res. Lett., 46, 8174– 8183. doi:10.1029/2019GL082182.

Studinger, M. (2014). IceBridge ATM L4 Surface Elevation Rate of Change, Version 299 1, Antarctica subset. N. S. a. I. D. C. D. A. A. Center. Boulder, Colorado, USA. doi:10.5067/BCW6CI3TXOCY.

Van Wessem, J. M., Reijmer, C. H., Morlighem, M., Mouginot, J., Rignot, E., Medley, B., Joughin, I., Wouters, B., Depoorter, M. A., Bamber, J. L., Lenaerts, J. T. M., De Van Berg, W. J., Van Den Broeke, M. R., & Van Meijgaard, E. (2014). Improved representation of East Antarctic surface mass balance in a regional atmospheric climate model. J. Glac., 60(222), 761–770. doi:10.3189/2014JoG14J051.

Velicogna, I., Mohajerani, Y., A, G., Landerer, F., Mouginot, J., Noel, B., Rignot, E., Sutterley, T., van den Broeke, M., van Wessem, J. M., & Wiese, D. (2020). Continuity of ice sheet mass loss in Greenland and Antarctica from the GRACE and GRACE Follow-On missions. Geophys. Res. Lett., 47(8). doi:10.1029/2020GL087291.

Zwally, H. Jay, Mario B. Giovinetto, Matthew A. Beckley, and Jack L. Saba, 2012, Antarctic and Greenland Drainage Systems, GSFC Cryospheric Sciences Laboratory, at http://icesat4.gsfc.nasa.gov/cryo_data/ant_grn_drainage_systems.php.